Probabilistic Tracklet Characterization and Prioritization Using Admissible Regions

Marcus J. Holzinger*
Georgia Institute of Technology
K. Kim Luu†, Chris Sabol†
Air Force Research Laboratory, USAF
Keric Hill‡
Integrity Applications Incorporated

Abstract

This paper introduces and discusses a method to rigorously classify and prioritize UCTs using Bayesian inference and admissible regions. A detailed derivation and discussion of the methodology is given, followed by a generalized definition of prioritization parameters. Several example prioritization parameters including 'time left to detect,' 'zero-effort miss,' and 'effective albedo-area' are motivated and given. A number of illustrative applications with optical UCTs are examined to demonstrate information that can be extracted from each observation. Finally, the information extracted from each UCT is then compared and approaches to observation prioritization discussed.

1 Introduction

Space Situational Awareness (SSA), the detection, tracking, and characterization of Space Objects (SOs), is needed to protect the United States and its allies and to maintain economic and diplomatic objectives.[1,2] The U.S. Strategic Command (USSTRATCOM) Joint Space Operations Center (JSpOC) operates the Space Surveillance Network (SSN) and currently tracks 17,000 objects with diameters greater than 10 cm, of which approximately 1,000 are active.[3,4] Presently, the majority of JSpOC SSN Space Object Catalog (SOC) maintenance is done using optical and radar measurements of space debris and active spacecraft.[5]

A central problem in constructing and maintaining the SOC is the allocation of relatively few sensor assets to the task of tracking the existing 17,000 objects (some of which maneuver without notice) as well as detecting & characterizing new objects. This task is confounded by the intuitive realization that one can only track and improve orbit estimates if the SO orbit is already known. Further, some space objects may have the potential to interact with on-orbit assets (e.g., collisions), necessitating further scrutiny and characterization. Thus, sensor asset tasks must be intelligently prioritized between searching, tracking, and characterization activities for new or lost SOs.

The problem of command and control of the SSN to detect and track SOs using information theoretic methods has received renewed interest in recent years, and has a rich body of theoretical literature (see Blackman,[6] Mahler,[7] and their cited literature). A selection of representative methods applied to the SSA detection & tracking problem include risk-based sensor tasking,[8] combined estimation / tracking approaches,[9] and Adaptive Entropy-based Gaussian-mixture Information Synthesis Finite Set Statistics (AEGIS-FISST) methods.[10] Each of these methods quantifies performance of the sensor allocation problem using measures of state uncertainty statistics and / or the risk that there are undetected SOs.

*Assistant Professor, School of Aerospace Engineering, AIAA Senior Member, 270 Ferst Dr., Atlanta, Georgia, 30332-0150
†USAF, Air Force Research Laboratory, Directed Energy Directorate; 535 Lipoa Parkway, Suite #200, Kihei, Hawaii 96753
‡Integrity Applications Incorporated, 1300 N Holopono St. Suite 116, Kihei, Hawaii 96753

Report Documentation Page

Form Approved
OMB No. 0704-0188

1. REPORT DATE	2. REPORT TYPE	3. DATES COVERED
SEP 2014		**00-00-2014 to 00-00-2014**

4. TITLE AND SUBTITLE	5a. CONTRACT NUMBER
Probabilistic Tracklet Characterization and Prioritization Using Admissible Regions	5b. GRANT NUMBER
	5c. PROGRAM ELEMENT NUMBER
6. AUTHOR(S)	5d. PROJECT NUMBER
	5e. TASK NUMBER
	5f. WORK UNIT NUMBER
7. PERFORMING ORGANIZATION NAME(S) AND ADDRESS(ES) **Air Force Research Laboratory,Directed Energy Directorate,535 Lipoa Parkway, Suite #200,Kihei,HI,96753**	8. PERFORMING ORGANIZATION REPORT NUMBER
9. SPONSORING/MONITORING AGENCY NAME(S) AND ADDRESS(ES)	10. SPONSOR/MONITOR'S ACRONYM(S)
	11. SPONSOR/MONITOR'S REPORT NUMBER(S)

12. DISTRIBUTION/AVAILABILITY STATEMENT
Approved for public release; distribution unlimited

13. SUPPLEMENTARY NOTES
In the Advanced Maui Optical and Space Surveillance Technologies (AMOS) Conference, 9-12 Sep 2014, Maui, HI.

14. ABSTRACT
This paper introduces and discusses a method to rigorously classify and prioritize UCTs using Bayesian inference and admissible regions. A detailed derivation and discussion of the methodology is given, followed by a generalized de nition of prioritization parameters. Several example prioritization parameters including 'time left to detect,' 'zero-e ort miss,' and 'e ective albedo-area' are motivated and given. A number of illustrative applications with optical UCTs are examined to demonstrate information that can be extracted from each observation. Finally, the information extracted from each UCT is then compared and approaches to observation prioritization discussed.

15. SUBJECT TERMS

16. SECURITY CLASSIFICATION OF:			17. LIMITATION OF ABSTRACT	18. NUMBER OF PAGES	19a. NAME OF RESPONSIBLE PERSON
a. REPORT **unclassified**	b. ABSTRACT **unclassified**	c. THIS PAGE **unclassified**	**Same as Report (SAR)**	**29**	

However, minimizing uncertainty in the dynamical states of the SO population is only one element of effective SSA. Because "... SSA involves characterizing, as completely as necessary, the space capabilities operating within the terrestrial environment and the space domain,[2]" the problem of allocating finite sensors to the tasks of SO detection, tracking, and characterization is inherently a high dimensional multi-objective optimization problem. Myopic approaches to minimize state uncertainty have no guarantees that sufficient observation resources will be allocated to objects that, for example, may a) pose collision risks, b) may not be found again unless immediate new observations are made, or c) necessitate non-dynamical characterization activities. This observation severely complicates the problem of SSN resource allocation.

Aside from emphasizing that the SSA resource allocation multi-objective optimization problem exists, this investigation does not presume to pose a specific solution approach to the problem. Rather, the scope of this investigation is to develop a rigorous, generalized framework to extract actionable information from an initial Uncorrelated Track (UCTs), generating necessary inputs to the SSA resource allocation problem. This subproblem is particularly troublesome, as with a single UCT, it is often not possible to uniquely identify the state of the object, or how useful it might be to immediately prioritize additional observations.

In operational reality, many observations of space objects take place over short periods of time or within small sensor fields of regard and do not possess sufficient geometric diversity to initiate well posed classical Initial Orbit Determination (IOD) algorithms. When a sequence of measurements (UCTs) cannot be associated with entities in the Space Object Catalog (SOC), operators are faced with the problem of determining the potential threat of the object and obtaining further measurements. The solution to this problem is confounded in scenarios with an overabundance of UCTs and limited sensor tasking availability. This investigation endeavors to rigorously provide actionable, attributable information on each UCT with which tasking decisions regarding followup observations may be made.

Admissible Region (AR, sometimes called Constrained Admissible Region - CAR) methods, i.e., methods to constrain undetermined states using *a-priori* constraint hypotheses, have been proposed to support data association and track initiation tasks. Well before their use in data association for asteroids and SOs, admissible regions have been used in stochastic economic modeling,[11] network traffic management for automated teller machines,[12] data association for consumer behavior prediction,[13] and fuzzy logic resource management.[14]

Milani et al.[15] first proposed using ARs to assist in the optical detection and discrimination of asteroids. This work is extended to SO detection and discrimination using both optical and radar measurements by Tommei et al.[16] More recently, the admissible region approach has been applied to SO detection and discrimination using time-resolved magnetometer measurements.[17] Recent efforts refine these approaches and make further advances in the association of multiple disparate UCTs.[18,19] While generating an admissible region does not give a specific initial state to initiate an estimator, it can be used to initialize an ensemble filter (particle filter or unscented particle filter) that approximates the admissible region as a uniform probability density function.[20]

This investigation builds upon these previous efforts by observing that, for each UCT, there is a) some phenomenological information that can be used to infer SO characteristics, and b) a continuum of discrete individual state hypotheses with a well defined probability density function composing the Admissible Region. By carefully examining this continuum of state hypotheses and phenomenological information while respecting the statistics of the admissible region probability distribution, it is possible to rigorously assign probabilities that a given SO possesses a specific orbit classification or generic prioritization parameter (e.g., 'time left to detect,' 'zero-effort miss to the International Space Station,' or 'albedo-area').

The specific contributions of this research effort are 1) The introduction and development of an approach to probabilistically classify a given UCT using the admissible region and Bayesian inference without *a-priori* knowledge, 2) The extension of the approach to condition the classification on *a-priori* knowledge of the distribution of possible UCT populations (such as the Space Object Catalog), 3) A method to verify whether a classification probability (with or without *a-priori* knowledge) is truly zero or the result of numerical implementation, and 4) The inclusion of UCT prioritization measures and approaches to generate attributable statistical measures to support UCT prioritization decisions.

This paper uses the following organization on its contents: §2 introduces the Admissible Region and

develops contributions 1, 2, and 3. §3 defines arbitrary prioritization parameter functions, statistical tests on such functions and details several candidate functions (contribution 4). §4 briefly reviews the construction of Admissible Regions for optical measurements, and §5 presents several scenarios demonstrating the utility of the approaches presented in this paper. Finally, §6 summarizes results and discusses impact of the approach.

2 Classification Approach

To generate the first three contributions of this investigation, Admissible Regions are formally developed and defined in the first subsection. Subsequent subsections then progress to demonstrate the primary contributions of this paper.

2.1 Review of Admissible Regions

The admissible region approach to initial orbit determination is discussed extensively in the literature.[15,16,18,21,17] However, notations often differ between sensor detection types (e.g., optical, radar, magnetometer) and from author to author. This subsection briefly introduces a unified notation (originally proposed by Worthy & Holzinger) and serves as a primer for the notation used in the main body of this investigation.

Consider a measurement phenomenology that corresponds to the measurement model

$$\mathbf{y} = \mathbf{h}(\mathbf{x}, t_k; \mathbf{k}) \tag{1}$$

where $\mathbf{y} \in \mathbb{R}^m$ is a measurement, $\mathbf{x} \in \mathbb{R}^n$ is the space object state, t_k is the time of the observation, and $\mathbf{k}$ is a set of additional relevant parameters. If $m < n$, $\mathbf{x}$ cannot be uniquely determined from $\mathbf{y}$, t_k, and $\mathbf{k} \in \mathbb{R}^p$. However, if $\mathbf{x}$ is properly chosen and partitioned such that, at time t_k,

$$\mathbf{x} = \begin{bmatrix} \mathbf{x}_d^T & \mathbf{x}_u^T \end{bmatrix}^T \tag{2}$$

where $\mathbf{x}_d \in \mathbb{R}^d$ $(d < n)$ are the states that can be uniquely determined, and $\mathbf{X}_u \in \mathbb{R}^u$, $(u + d = n)$ captures the undetermined states from the observation, then it must be true at time t_k that

$$\mathbf{x}_d = \mathbf{h}^{-1}(\mathbf{y}, \mathbf{x}_u, t_k; \mathbf{k}) \tag{3}$$

Given just the measurement information $\mathbf{y}$ at time t_k, $\mathbf{x}_u \in \mathbb{R}$ is entirely unconstrained. However, there are often reasonable conditions imposed on possible solutions $\mathbf{x}_u$ by the operators. These are generally introduced as a collection of inequality constraints on the solution $\mathbf{x}$ which may be represented in vector form as

$$\mathbf{g}(\mathbf{x}_d, \mathbf{x}_u, t_k; \mathbf{k}) \leq \mathbf{0} \tag{4}$$

where $\mathbf{g} : \mathbb{R}^d \times \mathbb{R}^u \times \mathbb{R} \times \mathbb{R}^p \to \mathbb{R}^l$. Then, substituting Eqn. (3) in to Eqn. (4) generates

$$\mathbf{g}(\mathbf{h}^{-1}(\mathbf{y}, \mathbf{x}_u, t_k; \mathbf{k}), \mathbf{x}_u, t_k; \mathbf{k}) = \boldsymbol{\kappa}(\mathbf{x}_u; t_k, \mathbf{y}, \mathbf{k}) \leq \mathbf{0} \tag{5}$$

These constraints $\boldsymbol{\kappa}(\mathbf{x}_u; \cdot) \leq \mathbf{0}$ on the undetermined states $\mathbf{x}_u$ are referred to as the Admissible Constraints. Any volume of space $\mathbf{x}_u \in \mathcal{A} \subseteq \mathbb{R}^u$ that satisfies $\boldsymbol{\kappa}(\mathbf{x}_u; \cdot) \leq \mathbf{0}$ is then said to be the Admissible Region (or the Constrained Admissible Region). More formally, the admissible region may be defined in set notation as

$$\mathcal{A} \equiv \{\mathbf{x}_u \in \mathbb{R}^u | \boldsymbol{\kappa}(\mathbf{x}_u; \cdot) \leq \mathbf{0}\} \tag{6}$$

There are three important observations that must be made here. The first is that each and every undetermined state $\mathbf{x}_u \in \mathcal{A}$, when combined with the determined states $\mathbf{x}_d \in \mathbb{R}^d$, forms a full state $\mathbf{x} \in \mathbb{R}^n$. The second observation is that all such states $\mathbf{x} = [\mathbf{x}_d^T \ \mathbf{x}_u]^T$ necessarily generate exactly the same measurement using the measurement model given in Eqn. (1). Lastly, it must be emphasized that the Admissible Region $\mathcal{A}$ is the set of admissible undetermined states $\mathbf{x}_u$ under the hypothesis that $\boldsymbol{\kappa}(\mathbf{x}_u; \cdot) \leq \mathbf{0}$ is true - the quality of this assumption most assuredly depends on the object in question.

To illustrate this last point, consider an optical observation of an asteroid. Given the measurements made, an admissible region can be constructed assuming that the object possesses a closed orbit about the Earth. This in turn will generate an Admissible Region $\mathcal{A}$, however all admissible points $\mathbf{x}_u \in \mathcal{A}$ cannot include the true asteroid state - the admissible hypothesis used to form $\mathcal{A}$, that $\boldsymbol{\kappa}(\mathbf{x}_u; \cdot) \leq \mathbf{0}$, is false.

Nevertheless, while care must be exercised, such scenarios can be handled using common hypothesis testing methods. The following subsection introduces the classification notation and approach constituting the primary contributions of this investigation.

2.2 Classification in the Admissible Region

Suppose that the undetermined state space Admissible Region $\mathcal{A}$ can be partitioned in to a finite set of disjoint sub volumes, each corresponding to a state classification of interest.

$$\mathcal{A}_1 \cup \cdots \cup \mathcal{A}_i \cup \cdots \cup \mathcal{A}_j \cup \cdots \cup \mathcal{A}_N \equiv \mathcal{A} \tag{7}$$

where $\mathcal{A}_i \cap \mathcal{A}_j = \varnothing \; \forall i \neq j$ and $\mathcal{A}$ is the set that contains all objects of interest (ex: Earth-orbiting objects). As with all probabilistic classification problems, it is common to include a 'none-of-the-above' (NOTA) classification to ensure that all of the classifications $\mathcal{A}_i$ span the parent set $\mathcal{A}$.

Next, a hypothesis H_i can be formed that an observed object with undetermined states $\mathbf{x}_u$ is a member of a given classification $\mathcal{A}_i$ under the condition that it is a member of the parent set $\mathcal{A}$.

$$H_i = \{\mathbf{x}_u \in \mathcal{A}_i | \mathbf{x}_u \in \mathcal{A}\} \tag{8}$$

To compute the probability that H_i is true, the random variable $\mathbf{X}_u \in \mathbb{R}^u$ from which any specific $\mathbf{x}_u$ is instantiated is introduced. Then, an application of Bayes Theorem produces

$$\mathbb{P}\left[H_i\right] = \mathbb{P}\left[\mathbf{X}_u \in \mathcal{A}_i | \mathbf{X}_u \in \mathcal{A}\right] = \frac{\mathbb{P}\left[\mathbf{X}_u \in \mathcal{A} | \mathbf{X}_u \in \mathcal{A}_i\right] \mathbb{P}\left[\mathbf{X}_u \in \mathcal{A}_i\right]}{\mathbb{P}\left[\mathbf{X}_u \in \mathcal{A}\right]} \tag{9}$$

Because $\mathcal{A}_i \subseteq \mathcal{A}$, $\mathbb{P}\left[\mathbf{X}_u \in \mathcal{A} | \mathbf{X}_u \in \mathcal{A}_i\right] = 1$. $\mathbb{P}\left[H_i\right]$ then simplifies to

$$\mathbb{P}\left[H_i\right] = \frac{\mathbb{P}\left[\mathbf{X}_u \in \mathcal{A}_i\right]}{\mathbb{P}\left[\mathbf{X}_u \in \mathcal{A}\right]} \tag{10}$$

To compute each of these probabilities of set membership, suppose that $\mathbf{X}_u$ has some probability density function (PDF) $f_{\mathcal{A}}(\mathbf{x}_u)$ that describes the probability density of $\mathbf{X}_u$ within $\mathcal{A} \subseteq \mathbb{R}^u$. Then, the probability that $\mathbf{X}_u \in \mathcal{A}$ can be computed using

$$\mathbb{P}\left[\mathbf{X}_u \in \mathcal{A}\right] = \int_{\mathcal{A}} f_{\mathcal{A}}(\mathbf{x}_u) \mathrm{d}\mathbf{x}_u \tag{11}$$

and similarly,

$$\mathbb{P}\left[\mathbf{X}_u \in \mathcal{A}_i\right] = \int_{\mathcal{A}_i} f_{\mathcal{A}}(\mathbf{x}_u) \mathrm{d}\mathbf{x}_u \tag{12}$$

If the PDF $f_{\mathcal{A}}(\mathbf{x}_u)$ is known, the probability $\mathbb{P}\left[H_i\right]$ may be computed using (10), (11), and (12). However, if no information exists to characterize probability distribution $f_{\mathcal{A}}(\mathbf{x}_u)$, then it must be the case that $f_{\mathcal{A}}(\mathbf{x}_u)$ is uniform over the state space volume of $\mathcal{A}$. Thus, (11) and (12) must necessarily become

$$\mathbb{P}\left[\mathbf{X}_u \in \mathcal{A}\right] = \int_{\mathcal{A}} k_{\mathcal{A}} U(\mathbf{x}_u) \mathrm{d}\mathbf{x}_u = k_{\mathcal{A}} \mathrm{Vol}(\mathcal{A}) \tag{13}$$

and

$$\mathbb{P}\left[\mathbf{X}_u \in \mathcal{A}_i\right] = \int_{\mathcal{A}_i} k_{\mathcal{A}} U(\mathbf{x}_u) \mathrm{d}\mathbf{x}_u = k_{\mathcal{A}} \mathrm{Vol}(\mathcal{A}_i) \tag{14}$$

where $k_{\mathcal{A}}$ is the value of the uniform density at any point in the volume of interest, $U(\mathbf{x}_u)$ is the uniform distribution, and the $\text{Vol}(\cdot)$ operator computes the total volume of the set of interest. Finally, $\mathbb{P}[H_i]$ can be computed as

$$\mathbb{P}[\mathbf{X}_u \in \mathcal{A}_i | \mathbf{X}_u \in \mathcal{A}] = \mathbb{P}[H_i] = \frac{\text{Vol}(\mathcal{A}_i)}{\text{Vol}(\mathcal{A})} \tag{15}$$

Because, as defined in (7), the sets $\mathcal{A}_i$, $i = 1, \ldots, N$ fully span the parent set $\mathcal{A}$, it must be true that

$$\sum_{i}^{N} \mathbb{P}[H_i] = 1 \tag{16}$$

The result given in (15) constitutes the first contribution of this investigation and bears further discussion. Firstly, it may be the case that many classifications $\mathcal{A}_i = \varnothing$. When this occurs there are no admissible states $\mathbf{x}_u \in \mathcal{A}$ that correspond to the classification $\mathcal{A}_i$. While at first this observation may appear uninformative, using the available measurement evidence $\mathbf{y}$ to eliminate possible classifications $\mathcal{A}_i$ has substantial utility, as in practice this step reduces the number of potential classification hypotheses H_i by a sizable factor. Second, it is common for some classification probabilities H_i to be quite small. This should not be taken as evidence that the classification $\mathcal{A}_i$ should be discarded - further measurements must be gathered to determine whether states $\mathbf{x}_u \in \mathbb{A}_i$ are consistent with available information.

In some scenarios, $f_{\mathcal{A}}(\mathbf{x}_u)$ is not known, but there is information available that describes the distribution of the full state information. The following subsection develops an approach to condition H_i on such information.

2.3 Conditional Hypotheses Using A-Priori Information

In the event that *a-priori* information $[\mathbf{X}_u^T \ \mathbf{X}_d^T]^T = \mathbf{X} \in \mathcal{C}$ is available, then the hypothesis H_i must be modified. This may be the case when it is known or assumed that the distribution of the full admissible region is well represented using known catalog information (e.g., the Space Object Catalog). In this case, the full state-space may be partitioned in to individual classification states such that $\mathcal{C}_1 \cup \cdots \cup \mathcal{C}_i \cup \cdots \cup \mathcal{C}_j \cup \cdots \cup \mathcal{C}_N \equiv \mathcal{C}$, much like the admissible region sets comprising $\mathcal{A}$. Under such a partition, the set $\mathcal{A}_j$ is generated when the measurements $\mathbf{x}_d$ are imposed on $\mathcal{C}_j$. With this definition, some sets $\mathcal{C}_j$ are not compatible with evidence $\mathbf{x}_d$, yielding $\mathcal{A}_j = \varnothing$. The hypothesis H_i conditioned on $\mathbf{X} \in \mathcal{C}$ is

$$\begin{aligned} \mathbb{P}[H_i | \mathbf{X} \in \mathcal{C}] = \mathbb{P}[H_{i,ap}] &= \mathbb{P}[\mathbf{X}_u \in \mathcal{A}_i | (\mathbf{X}_u \in \mathcal{A}) \cap (\mathbf{X} \in \mathcal{C})] \\ &= \mathbb{P}[(\mathbf{X}_u \in \mathcal{A}_i | \mathbf{X}_u \in \mathcal{A}) \cap (\mathbf{X}_u \in \mathcal{A}_i | \mathbf{X} \in \mathcal{C})] \end{aligned} \tag{17}$$

Because, by definition,

$$\mathbb{P}[\mathbf{X}_u \in \mathcal{A}_i] \equiv \mathbb{P}[\mathbf{X} \in \mathcal{C}_i | \mathbf{x}_d] \tag{18}$$

It can be shown that

$$(\mathbf{X}_u \in \mathcal{A}_i | \mathbf{X} \in \mathcal{C}) \Rightarrow (\mathbf{X} \in \mathcal{C}_i | \mathbf{X} \in \mathcal{C}) \tag{19}$$

Hence, using this result combined with Bayes Theorem,

$$\mathbb{P}[H_{i,ap}] = \mathbb{P}[(\mathbf{X}_u \in \mathcal{A}_i | \mathbf{X}_u \in \mathcal{A}) \cap (\mathbf{X} \in \mathcal{C}_i | \mathbf{X} \in \mathcal{C})] \tag{20}$$

$$= \mathbb{P}[(\mathbf{X}_u \in \mathcal{A}_i) \cap (\mathbf{X} \in \mathcal{C}_i) \,|\, (\mathbf{X}_u \in \mathcal{A}) \cap (\mathbf{X} \in \mathcal{C})] \tag{21}$$

$$= \frac{\mathbb{P}[(\mathbf{X}_u \in \mathcal{A}) \cap (\mathbf{X} \in \mathcal{C}) \,|\, (\mathbf{X}_u \in \mathcal{A}_i) \cap (\mathbf{X} \in \mathcal{C}_i)] \, \mathbb{P}[(\mathbf{X}_u \in \mathcal{A}_i) \cap (\mathbf{X} \in \mathcal{C}_i)]}{\mathbb{P}[(\mathbf{X}_u \in \mathcal{A}) \cap (\mathbf{X} \in \mathcal{C})]} \tag{22}$$

Because $\mathcal{A}_i \subseteq \mathcal{A}$ and $\mathcal{C}_i \subseteq \mathcal{C}$, the first term in the numerator simplifies to unity. Then,

$$\mathbb{P}[H_{i,ap}] = \frac{\mathbb{P}[(\mathbf{X}_u \in \mathcal{A}_i) \cap (\mathbf{X} \in \mathcal{C}_i)]}{\mathbb{P}[(\mathbf{X}_u \in \mathcal{A}) \cap (\mathbf{X} \in \mathcal{C})]} \tag{23}$$

$$= \frac{\mathbb{P}[\mathbf{X}_u \in \mathcal{A}_i] \, \mathbb{P}[\mathbf{X} \in \mathcal{C}_i]}{\sum_{j=1}^{N} \sum_{m=1}^{N} \mathbb{P}[\mathbf{X}_u \in \mathcal{A}_j] \, \mathbb{P}[\mathbf{X} \in \mathcal{C}_m]} \tag{24}$$

Since $\mathcal{C}_m$ conditioned on a measured $\mathbf{x}_d$ is exactly $\mathcal{A}_m$, all terms in which $j \neq m$ disappear, giving the form

$$\mathbb{P}\left[H_{i,ap}\right] = \frac{\mathbb{P}\left[\mathbf{X}_u \in \mathcal{A}_i\right]\mathbb{P}\left[\mathbf{X} \in \mathcal{C}_i\right]}{\sum_{j=1}^{N}\mathbb{P}\left[\mathbf{X}_u \in \mathcal{A}_j\right]\mathbb{P}\left[\mathbf{X} \in \mathcal{C}_j\right]} \tag{25}$$

Defining $f_{\mathcal{A}}(\mathbf{x}_u)$ and $f_{\mathcal{C}}(\mathbf{x})$ as the probability density functions over $\mathcal{A}$ and $\mathcal{C}$, respectively, the final form of the hypothesis probability is given

$$\mathbb{P}\left[H_{i,ap}\right] = \frac{\left(\int_{\mathcal{A}_i} f_{\mathcal{A}}(\mathbf{x}_u)\mathrm{d}\mathbf{x}_u\right)\left(\int_{\mathcal{C}_i} f_{\mathcal{C}}(\mathbf{x})\mathrm{d}\mathbf{x}\right)}{\sum_{j=1}^{N}\left(\int_{\mathcal{A}_j} f_{\mathcal{A}}(\mathbf{x}_u)\mathrm{d}\mathbf{x}_u\right)\left(\int_{\mathcal{C}_j} f_{\mathcal{C}}(\mathbf{x})\mathrm{d}\mathbf{x}\right)} \tag{26}$$

Again, it follows that

$$\sum_{i=1}^{N} H_{i,ap} = 1 \tag{27}$$

The result in Eqn. (26) is general to this point, and is correct for arbitrary probability densities. Under the simplifying assumption that the probability densities of $\mathbf{X}_u$ and $\mathbf{X}$ are uniform over each region $\mathcal{A}$ and $\mathcal{C}_i$, further simplification reveals that

$$\mathbb{P}\left[H_{i,ap}\right] = \frac{\left(\int_{\mathcal{A}_i} k_{\mathcal{A}}U(\mathbf{x}_u)\mathrm{d}\mathbf{x}_u\right)\left(\int_{\mathcal{C}_i} k_{\mathcal{C},i}U(\mathbf{x})\mathrm{d}\mathbf{x}\right)}{\sum_{j=1}^{N}\left(\int_{\mathcal{A}_j} k_{\mathcal{A}}U(\mathbf{x}_u)\mathrm{d}\mathbf{x}_u\right)\left(\int_{\mathcal{C}_j} k_{\mathcal{C},j}U(\mathbf{x})\mathrm{d}\mathbf{x}\right)} \tag{28}$$

$$= \frac{k_{\mathcal{A}}\mathrm{Vol}(\mathcal{A}_i)k_{\mathcal{C},i}\mathrm{Vol}(\mathcal{C}_i)}{\sum_{j=1}^{N} k_{\mathcal{A}}\mathrm{Vol}(\mathcal{A}_j)k_{\mathcal{C},j}\mathrm{Vol}(\mathcal{C}_j)} \tag{29}$$

which provides

$$\mathbb{P}\left[H_{i,ap}\right] = \frac{k_{\mathcal{C},i}\mathrm{Vol}(\mathcal{A}_i)\mathrm{Vol}(\mathcal{C}_i)}{\sum_{j=1}^{N} k_{\mathcal{C},j}\mathrm{Vol}(\mathcal{A}_j)\mathrm{Vol}(\mathcal{C}_j)} \tag{30}$$

While it may appear that assuming uniform probability densities over $\mathcal{A}$ and $\mathcal{C}_i$, $i = 1, \ldots, N$, is restrictive, as N increases the collection of regions, each with uniform distributions, can approximate more arbitrary probability distributions. Further, since the objective of the approach is to classify the admissible states $\mathbf{X}_u \in \mathcal{A}$, in practical applications it may be enough to define a sufficiently large number of classifications such that the piecewise uniform approximation is appropriate. Either the general form in Eqn. (26) or the simplified form in Eqn. (30) may be used, depending on the application. In UCT prioritization applications, the time available to make a decision based on classification information is sometimes very short, however, making Eqn. (30) an attractive option. With the classification hypotheses probability $H_{i,ap}$ conditioned on state space object density being defined, the second contribution of this investigation is demonstrated. The following subsection discusses specific application related issues when using a space object catalog as the it a-priori information.

2.4 Classification Approach and Space Object Catalogs

A space object catalog is an ideal collection of data to use as *a-priori* information when classifying space objects that are likely to be well represented as members of the space object catalog. In this case, a classification hierarchy may be defined and used to generate $\mathcal{C}_i$, $i = 1, \ldots, N$. Under such an approach, a given space object catalog may be subjected to a classification algorithm to empirically compute the densities $k_{\mathcal{C},i}$ used in Eqn. (10). This exact methodology is used in the Simulated Results section (§5) to generate *a-priori* conditioned classification hypotheses.

It must be emphasized that the conditioned hypothesis $H_{i,ap}$ should only be used if it is assumed that the SO in question is well represented as a member of the existing space object catalog. If the SO is not well represented by the space object catalog (e.g., under-observed orbit regimes, new objects), then the classification hypothesis H_i without the a-priori information may be more appropriate.

2.5 Vanishing Classification Probability Test

Depending on the approach used to construct the disjoint state classifications $\mathcal{C}_1 \cup \cdots \cup \mathcal{C}_N = \mathcal{C}$, it may be the case that a numerical implementation computing $\mathbb{P}[H_i]$ using Eqn. (15) or $\mathbb{P}[H_{i,ap}]$ using Eqn. (26) results in zero probability. However, to verify that this probability is not the result of insufficient discretization or sampling used to numerically compute (15) or (26), it may be good practice to confirm whether $\mathbb{P}[H_i] = 0$ ($\mathbb{P}[H_{i,ap}] = 0$) or whether the probability is simply below the level that a given numerical discretization or sampling method can detect. Said differently, a test must be developed to determine whether $\mathcal{A}_i = \varnothing$ or whether $\mathcal{A}_i$ is simply a very small region in $\mathcal{A}$.

One approach to demonstrate that $\mathcal{A}_i \neq \varnothing$ is to find at least one undetermined state $\mathbf{x}_u \in \mathcal{A}_i \subseteq \mathcal{A}$. If such a subspace state $\mathbf{x}_u$ can be found, then it is necessarily true that at least one admissible state exists that belongs to $\mathcal{C}_i$. The problem is now to develop a method to compute admissible values of $\mathbf{x}_u \in \mathcal{A}_i$. The first test to evaluate is whether the known state space values $\mathbf{x}_d$ (generated from $\mathbf{y}$, $\mathbf{k}$, and t_k) are consistent with $\mathcal{C}_i$. If $\mathbf{x}_d$ is inconsistent with $\mathcal{C}_i$, then $\mathcal{A}_i$ is truly empty ($= \varnothing$). However, if $\mathbf{x}_d$ is consistent with $\mathbf{C}_i$, then there may be at least one valid $\mathbf{x}_u \in \mathcal{A}_i \subseteq \mathcal{A}$.

The method to compute such a $\mathbf{x}_u$ is quite similar to the Admissible Region method in general. Given the known $\mathbf{x}_d$, the volume of space $\mathbf{x}_u$ that composes the membership of classification $\mathcal{C}_i$ can be computed as

$$\mathcal{C}_{i,u} \equiv \{\mathbf{x}_u \in \mathbb{R}^u | \mathbf{x}_u, \, \mathbf{x}_u \text{ consistent with } \mathcal{C}_i\} \tag{31}$$

Thus, $\mathcal{C}_{i,u} \in \mathbb{R}^u$, just as $\mathcal{A} \in \mathbb{R}^u$. Intuitively, if $\mathcal{C}_{i,u}$ intersects with $\mathcal{A}$, then there must be at least one $\mathbf{x}_u \in \mathcal{A}_i \subseteq \mathcal{A}$. Equivalently, this forces the natural result that

$$\mathcal{A}_i \equiv \mathcal{A} \cap \mathcal{C}_{i,u} \tag{32}$$

This identity is illustrated in Figure 1. There are three possible intersection cases between $\mathcal{A}$ and $\mathcal{C}_{i,u}$.

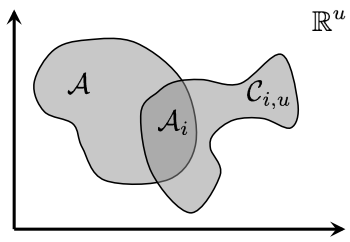

Figure 1: Illustration of $\mathcal{A} \cap \mathcal{C}_{i,u} \equiv \mathcal{A}_i \subseteq \mathcal{A} \subseteq \mathbb{R}^u$

1. $\mathcal{A} \cap \mathcal{C}_{i,u} = \varnothing \Rightarrow$ there are no admissible $\mathbf{x}_u \in \mathcal{A}_i$.
2. $(\mathcal{A} \cap \mathcal{C}_{i,u} \neq \varnothing)$ and $(0 \leq \dim \mathcal{A} \cap \mathcal{C}_{i,u} = u - 1) \Rightarrow$ there is only an intersection over a subspace of $\mathbb{R}^u$ where $\mathbf{x}_u$ is in both sets. While $\mathcal{A}_i \neq \varnothing$ and $\exists \mathbf{x}_u \in \mathcal{A}_i \subseteq \mathcal{A}$, the intersection subspace has precisely zero volume when integrated over the admissible region $\mathcal{A}_i \subseteq \mathbb{R}^u$, causing all such integrals to vanish. Thus any set membership hypothesis must also have zero probability (e.g., $\mathbb{P}[H_i] = \mathbb{P}[H_{i,ap}] = 0$).
3. $(\mathcal{A} \cap \mathcal{C}_{i,u} \neq \varnothing)$ and $(\dim \mathcal{A} \cap \mathcal{C}_{i,u} = u) \Rightarrow$ there is a an intersection in $\mathbb{R}^u$ such that a volume integral over $\mathcal{A}_i \subseteq \mathbb{R}^u$ is non-zero (however small).

In general, most intersections will correspond to case 1 or case 3. Now, consider possible numerical methods to generate $\mathcal{A}_i \subseteq \mathbb{R}^u$. A direct analytical computation method to generate $\mathcal{A} \cap \mathcal{C}_{i,u}$ is quite difficult and depends greatly on the admissible region $\mathcal{A}$ and the admissible classification states $\mathcal{C}_{i,u}$. However, a simple numerical approach is to discretize or sample particles from the set $\mathcal{C}_{i,u}$. Then, for each point or particle $\mathbf{x}_u \in \mathcal{C}_{i,u}$, compute whether $\mathbf{x}_u \in \mathcal{A}$ by evaluating the inequalities $\boldsymbol{\kappa}(\mathbf{x}_u; \cdot) \leq \mathbf{0}$ The resulting spread of admissible discrete $\mathbf{x}_u$ can the be evaluated to determine whether there is no intersection, intersection over a subspace, or intersection over $\mathbb{R}^u$.

3 Distributions of Prioritization Decision Parameters

Since every admissible point $\mathbf{x}_u \sim \mathbf{X}_u \in \mathcal{A}$ is consistent with the collected measurements forming $\mathbf{x}_d$, each $\mathbf{x} = \left[\mathbf{x}_u^T \ \mathbf{x}_d^T\right]^T$ may be considered a candidate state hypothesis drawn from the random variable $\mathbf{X} = \left[\mathbf{X}_u^T \ \mathbf{x}_d^T\right]^T$. In a manner similar to the classification approach discussed in §2, knowledge of the distribution of $\mathbf{X}_u$ may be used to compute distributions of decision parameters that serve as inputs to prioritization schemes. This section develops the third contribution of this effort. Suppose that the following arbitrary mapping function

$$m = \mu\left(\mathbf{x}_u; \mathbf{x}_d, \mathbf{y}, \mathbf{k}, t\right) \tag{33}$$

computes the decision parameter m given the a specific realization of $\mathbf{x}_u$, the determined state partition $\mathbf{x}_d$, observed information $\mathbf{y}$, arbitrary parameters $\mathbf{k}$, and decision time t. When $\mathbf{X}_u$ is allowed to be a random variable, then

$$M = \mu\left(\mathbf{X}_u; \mathbf{x}_d, \mathbf{y}, \mathbf{k}, t\right) \tag{34}$$

Generates the resulting random variable representing the random decision parameter M. This random function can be conditioned on *a-priori* information (e.g., $\mathbf{X} \in \mathcal{C}$) and / or examined under the assumption that $\mathbf{X}_u \in \mathcal{A}_i$, depending on the user's objectives. In general, the mapping function μ may be nonlinear and even discontinuous, making a thorough analytical characterization of arbitrary M out of scope for this investigation. Regardless, because the continuum of states in the admissible region $\mathcal{A}$ (and by extension $\mathcal{A}_i$) may be realized, the probability density function and cumulative distribution function of M may be numerically computed and tested using statistical methods. Short outlines of several possible methods are briefly discussed.

3.1 Minimum / Maximum Value Probability Thresholds

Because M is a random variable, one approach to using it to inform prioritization decisions is to compute the probability that its value lies within minimum and/or maximum bounds. To do so, given specific minimum and maximum values m_l and m_u, respectively, one computes

$$\mathbb{P}\left[m_l \leq M \leq m_u\right] = \int_{m_l}^{m_u} f_\mu(m)\mathrm{d}m \tag{35}$$

where m_l, m_u, or both must be defined. The probability density of M, $f_\mu(m)$, is computed analytically if possible, or empirically if practical.

3.2 Confidence Level Thresholds

Rather than commuting the probability that the performance factor is above, below, or between specified thresholds, one may alternately specify a confidence probability threshold for an inequality. In particular, because the cumulative distribution function is non-decreasing, if it is smooth then

$$m_{\text{th}} = \arg\left(\mathbb{P}\left[M \leq m\right] = p_{\text{th}}\right) \tag{36}$$

where $p_{\text{th}} \in (0, 1)$ is a specified probability threshold, and m_{th} is the value at which this probability threshold is met.

3.3 Example Decision Parameter: Time Left to Detect

When scheduling sensor tasks it is sometimes useful to know how much longer a specific UCT may be available for observation. To probabilistically determine how much time is left in which the object may be detected (the 'time left to detect'), various detection loss modes must be modeled and the minimum time at which the signal may be lost identified. For optical systems, transit of a space object in to eclipse or out of

the sensor platform line-of-sight are reasonable detection loss modes. If the SO position $\mathbf{r}(t) = \mathbf{r}(t; \mathbf{x}_u, \mathbf{x}_d, t_0)$, then the time to eclipse is defined as

$$t_{\text{eclipse}}(\mathbf{x}_u, \mathbf{x}_d, \hat{\mathbf{s}}(t), t_0) = \arg \min_{t \in [t_0, \infty)} \{\hat{\mathbf{s}}(t) \cdot \mathbf{r}(t) > 0 \cap \hat{\mathbf{s}}(t) \times \mathbf{r}(t) = R_e\} \tag{37}$$

where $\hat{\mathbf{s}}(t)$ is the sun unit vector. Time to sensor LOS loss is dependent on the sensor in question. If the only limitation on the sensor is whether the Earth blocks the light of sight, then defining $\mathbf{o}(t) = \mathbf{o}(t; \mathbf{x}_u, \mathbf{x}_d, t_0)$,

$$t_{\text{LOS}}(\mathbf{x}_u, \mathbf{x}_d, t_0) = \arg \min_{t \in [t_0, \infty)} \left\{ \left\| \mathbf{o}(t) + \left[\mathbf{o}(t)^T \left(\frac{\mathbf{r}(t) - \mathbf{o}(t)}{\|\mathbf{r}(t) - \mathbf{o}(t)\|} \right) \right] \left(\frac{\mathbf{r}(t) - \mathbf{o}(t)}{\|\mathbf{r}(t) - \mathbf{o}(t)\|} \right) \right\| = R_e \right\} \tag{38}$$

Then, the performance parameter t_{LTD} capturing the "time left to detect" is defined:

$$t_{\text{LTD}}(t; \mathbf{x}_u, \mathbf{x}_d, \hat{\mathbf{s}}(t), t_0) = \min_{t \in [t_0, \infty)} \{t_{\text{eclipse}}(t; \mathbf{x}_u, \mathbf{x}_d, \hat{\mathbf{s}}(t), t_0), t_{\text{LOS}}(\mathbf{x}_u, \mathbf{x}_d, t_0)\} \tag{39}$$

For this decision parameter, one could use either threshold probabilities or confidence level thresholds to inform prioritization decisions. For example, the probability that at least 10 seconds remain to detect the object can be computed.

3.4 Example Decision Parameter: Zero-Effort Miss

A chief SSA concern is the prediction and avoidance of on-orbit collision events. The Zero-Effort Miss (ZEM) distance between the detected SO and an Object Of Interest (OI) can be computed for each state hypothesis and statistics on the ZEM distance compiled. Supposing that the OI state $\mathbf{r}_{\text{OI}}(t) = \mathbf{r}_{\text{OI}}(t, \mathbf{x}_{\text{OI}}, t_0)$, the ZEM distance is simply

$$d_{\text{ZEM}} = \arg \min_{d, \text{ s.t.} t \in [t_0, \infty)} d = \|\mathbf{r}_{\text{OI}}(t) - \mathbf{r}(t)\| \tag{40}$$

Statistics on d_{ZEM} can be used to motivate additional followup observations to complete the initial orbit determination problem and identify whether a collision may occur.

3.5 Example Decision Parameter: Albedo-Area Product

Operationally, it is useful to characterize a new UCT by quantifying a measure of the SO size. An approximate measure related to SO size is the albedo-area ρA. Here, $\rho \in [0, 1]$ is the SO albedo (a measure of how much illumination is reflected from the surface to the observer) and A is the instantaneous illuminated area as seen by the observer. Optical sensors are capable of recording the brightness of an observed SO, and may report this as the SO apparent magnitude. The apparent magnitude as viewed by the observer is computed using

$$m_v = -\frac{5}{2} \log_{10} \left(\frac{I_{\text{sun}}}{d^2} \rho A \right) - 26.74 \tag{41}$$

Where I_{sun} is the illumination flux of the Sun at the SO (often in W/m^2) and d is the distance between the observer and the SO. Under the assumption that the SO distance from the sun is approximately the same as the observer distance from the sun, then inverting this function to solve for the albedo-area product ρA yields

$$\rho A = \left(\frac{d^2}{I_{\text{sun}}} \right) 10^{-\frac{2}{5}(m_v + 26.74)} \tag{42}$$

Unfortunately, only the product ρA may be quantified using this approach. If either ρ or A are known, then the remaining parameter may be computed. It should be noted, however, that for SOs a typical albedo value is $\rho = 0.175$.[22] This value is a global averaged albedo, and will not be the case in general, particularly if the SO is glinting.

3.6 Discussion on Uncorrelated Track Prioritization

As motivated in the introduction, a myopic focus in improving SO or SOC uncertainty does not address all SSA needs. The very nature of the SSA problem as a multiple objective optimization problem ensures that there is no single 'right' answer for the correct sensor tasking. Depending on strategic and tactical SSA needs, it may well be the case that the SO classification or a specific prioritization metric probabilities supersede the straightforward objective of reducing uncertainty.

As a concrete example, consider the Low Inclination Low Earth Orbit (LILO) SSA problem[23] which has specific objectives within the general SSA problem. Here, detecting and tracking LILO objects (maximum altitude less than 2,000km, inclination below 20°or greater than 160°) is the primary objective, so sensor observation priority should be given to UCTs that have high probabilities of being LILO objects. Supposing that multiple high-probability LILO objects are simultaneously tracked, additional prioritization metrics such as 'time left to detect' can be used to prioritize observations.

4 Admissible Regions for Optical Sensors

The preceding results do not assume any specific sensor phenomenology, and may be applied to general space object observations. Before presenting results, the approach to constructing Admissible Regions for optical space object measurements is briefly reviewed here. Figure 2 illustrates the geometry of the problem. An observer with position $\mathbf{o}$ and velocity $\dot{\mathbf{o}}$ collects measurements on a space object with position $\mathbf{r}$ and velocity $\dot{\mathbf{r}}$ at time t.

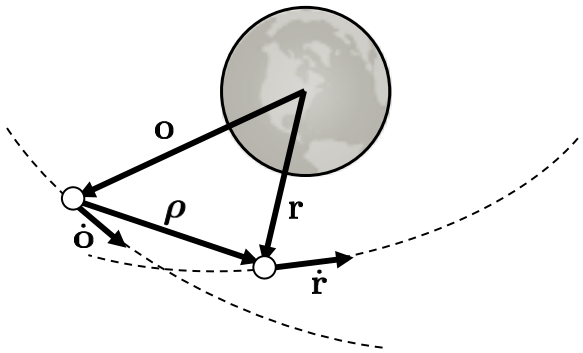

Figure 2: Observer and Space Object Geometry

The relative distance vector $\boldsymbol{\rho}$ and velocity vector $\dot{\boldsymbol{\rho}}$ are then

$$\boldsymbol{\rho} = \mathbf{r} - \mathbf{o} \tag{43}$$

$$\dot{\boldsymbol{\rho}} = \dot{\mathbf{r}} - \dot{\mathbf{o}} \tag{44}$$

Because optical measurements may only capture the line-of-sight bearing (often expressed in inertial coordinates) and cannot measure range, the relative distance vector is expressed as

$$\boldsymbol{\rho} = \rho \hat{\mathbf{l}}(\alpha, \beta) \tag{45}$$

where $\rho \geq 0$ is the relative range to the object from the observer, α is commonly the Right Ascension (RA), β is the Declination (DE), and

$$\hat{\mathbf{l}}(\alpha, \beta) = \begin{bmatrix} \cos\alpha \cos\beta \\ \sin\alpha \cos\beta \\ \sin\beta \end{bmatrix} \tag{46}$$

Using these definitions,

$$\frac{\mathrm{d}}{\mathrm{d}t}\boldsymbol{\rho} = \dot{\boldsymbol{\rho}} = \frac{\mathrm{d}\rho}{\mathrm{d}t}\hat{\mathbf{l}}(\alpha,\beta) + \rho\left[\frac{\partial\hat{\mathbf{l}}}{\partial\alpha}\frac{\mathrm{d}\alpha}{\mathrm{d}t} + \frac{\partial\hat{\mathbf{l}}}{\partial\beta}\frac{\mathrm{d}\beta}{\mathrm{d}t}\right] \tag{47}$$

$$= \dot{\rho}\hat{\mathbf{l}}(\alpha,\beta) + \rho\left[\hat{\mathbf{l}}_\alpha(\alpha,\beta)\dot{\alpha} + \hat{\mathbf{l}}_\beta(\alpha,\beta)\dot{\beta}\right] \tag{48}$$

Therefore, given the known observer location $\mathbf{o}$ and velocity $\dot{\mathbf{o}}$, given measurements α, β, $\dot{\alpha}$, and $\dot{\beta}$, (45) and (48) may be used to construct admissible positions $\mathbf{r}$ and velocities $\dot{\mathbf{r}}$ of the observed space object. All that is required is a hypothesis of the range ρ and range-rate $\dot{\rho}$ of the space object relative to the observer. In this formulation,

$$\mathbf{x}_d = \begin{bmatrix} \alpha & \beta & \dot{\alpha} & \dot{\beta} \end{bmatrix}^T \tag{49}$$

and

$$\mathbf{x}_u = \begin{bmatrix} \rho & \dot{\rho} \end{bmatrix}^T \tag{50}$$

To bound possible values of ρ and $\dot{\rho}$ and generate an admissible region $\mathcal{A}$, several constraints are defined. The first is the mass-specific energy relative to Earth (first imposed by Milani,[15] given as

$$g_1(\mathbf{x}_u) = \varepsilon(\mathbf{r}(\rho), \dot{\mathbf{r}}(\rho,\dot{\rho})) \leq 0 \tag{51}$$

The energy constraint in (51) essentially requires that the space object orbit be closed about the Earth, and assumes Keplerian motion. The second constraint used in this paper requires that the radius of periapsis be above the surface of the Earth:

$$g_2(\mathbf{x}_u) = R_e - r_p(\rho,\dot{\rho}) \leq 0 \tag{52}$$

Finally, the third constraint imposed on the admissible region is that of illumination (first proposed by Worthy, et al.). Because visible band optical sensors are being used in §5, it is required that the space object be illuminated by the sun.

$$g_3(\mathbf{x}_u) = R_e - \hat{\mathbf{s}} \times \mathbf{r}(\rho,\dot{\rho}) \leq 0 \text{ if } \hat{\mathbf{s}} \cdot \mathbf{r}(\rho,\dot{\rho}) > 0 \tag{53}$$

where $\hat{\mathbf{s}}$ is the illumination direction unit vector. Combined, g_1, g_2, and g_3 form $\mathbf{g}(\mathbf{x}_u) \leq \mathbf{0}$, which in turn formally define the admissible region $\mathcal{A}$.

5 Simulated Results

From a short sequence of inertial bearing measurements to the detected SO from the observer location $\mathbf{o}$, the apparent right ascension and declination (and their rates) can be approximated at time t as It should be emphasized that any state $\mathbf{x} = \begin{bmatrix} \mathbf{x}_d^T & \mathbf{x}_u^T \end{bmatrix}^T$ corresponds to a single deterministic orbit; no other choice of $\mathbf{x}_u$ can generate the same orbit.

5.1 Generation of A-Priori Information using The Space Object Catalog

The Joint Space Operations Center (JSpOC) Space Object Catalog* is used as *a-priori* information for the simulated results in this effort. The Space Object Catalog is ingested and classified according to the hierarchy outlined in Table 1. The classification is interpreted as a line-by-line 'if-elseif' logic (in the order shown), ensuring that each of the orbit classifications $\mathcal{C}_i$ are both disjoint and span the full orbit space $\mathcal{C}$. The classification approach developed here is not comprehensive and should be considered approximate; it serves to demonstrate how a more complete and rigorous classification methodology may be generated depending on user requirements.

Applying the classification methodology depicted in Table 1 gives the number of object entries under each classification listed in Table 2. The probability that a randomly drawn Space Object Catalog object possesses a specific classification $\mathcal{C}_i$ ($\mathbb{P}[\mathbf{X} \in \mathcal{C}_i|\mathrm{SOC}]$) is also given.

*`www.space-track.org`, accessed 2014/05/27

Table 1: Classification Methodology

Classification ($\mathcal{C}_i$)	Periapse Min/Max (km)	Apoapse Min/Max (km)	Eccentricity Min/Max	Inclination Min/Max (deg)
LEO:polar	R_e/-	-/R_e + 2,000	-/-	75/120
LEO:LILO	R_e/-	-/R_e + 2,000	-/-	0/20
LEO:NOTA	R_e/-	-/R_e + 2,000	-/-	-
Molniya	R_e/15,000	37,000/48,000	-/-	60/75
GTO:NOTA	R_e/10,000	-/50,000	-/-	-/75
or	10,000/40,000	35,000/45,000	-/-	-/75
MEO:low	R_e/-	-/10,000	-/-	-/-
MEO:subsynch	23,000/-	-/32,000	-/-	45/75
MEO:NOTA	10,000/-	-/40,000	-/0.1	-/-
GEO:slot	$R_{\text{GEO}} - 50$/-	-/$R_{\text{GEO}} + 50$	-/-	-/20
GEO:graveyard	$R_{\text{GEO}} + 50$/-	-/45,000	-/-	0/20
GEO:NOTA	40,000/-	-/45,000	-/-	0/20
HEO:NOTA	45,000/-	-/-	-/-	-/-
NOTA	-/-	-/-	-/-	-/-

Table 2: Space Object Catalog Classification Statistics

Classification ($\mathcal{C}_i$)	SOC Entries	$\mathbb{P}[\mathbf{X} \in \mathcal{C}_i \vert \text{SOC}]$
LEO:polar	7642	0.5142
LEO:LILO	17	0.0011
LEO:NOTA	3701	0.2490
Molniya:NOTA	274	0.0184
GTO:NOTA	1531	0.1030
MEO:low	123	0.0083
MEO:subsynch	261	0.0176
MEO:NOTA	33	0.0022
GEO:slot	476	0.0320
GEO:graveyard	235	0.0158
GEO:NOTA	411	0.0277
HEO:NOTA	75	0.0050
NOTA	83	0.0056
Total	14862	1.0000

5.2 Scenario Description

The observing site is assumed here to be the Advanced Electro-Optical System (AEOS) on Maui, Hawaii, located at 20.708 deg N, 203.743 deg E, 3075m altitude. At 06:42:02 UT on June 15, 2014, several objects described in Table 3 are considered to be detected (potentially by multiple sensors). Each object is assumed to have inertial bearing angle and angle-rate measurements extracted from sensors (e.g., streaks, multiple measurements over short time periods). The true orbit and classification of each detected space object is given in classical orbit elements at the detection time epoch, where a is the semi-major axis, e is the eccentricity, i is the inclination, Ω is the longitude of the ascending node, ω is the argument of periapsis, and f is the true anomaly. Each For the purposes of this illustration each detection is handled and discussed in the following subsections.

The objective of the following subsections is to apply the classification method (with and without assumed SOC membership defined in Tables 1 and 2). Additionally, the prioritization metrics defined in §3 for 'time left to detect,' 'zero-effort miss', and 'albedo-area' are computed both for the entire admissible region as well as for each classification. For each scenario a brief discussion is given, with a more complete discussion

Table 3: Test Case & Detected Object Descriptions

Case	Description	a (km)	e ()	i (deg)	Ω (deg)	ω (deg)	f (deg)
1	LEO, polar	7,153	0.00012	97	38	32	113
2	LEO, equatorial	6,978	0.00030	13	56	43	101
3	MEO	30,000	0.00020	53	62	41	132
4	GTO	24,471	0.73200	23.7	56	43	101
5	GEO	42,164	0.00005	7	38	32	113
6	Molniya	24,471	0.72300	63.4	38	212	287

reserved for digesting the generated statistics and considering possible prioritization schemes. A visualization of each UCT true orbit and observing geometry is also given (Figures 3, 5, 7, 9, 11, and 13). In each of these figures, the green star is the observing optical telescope location (AEOS), the red triangle is the true space object location at the time of detection, and the red line is the true orbit of the space object.

5.3 UCT 1: Polar Orbiting LEO Object

Polar orbiting LEO objects constitute the bulk of the Space Object Catalog, and as a result often generate UCTs. The admissible region generated by the observation is depicted in Figure 4(a) and the resulting histograms & CDFs for the 'Time Left-to-Detect,' 'Zero-Effort Miss,' and 'Albedo-Area' prioritization parameters are shown in Figures 4(b), 4(c), and 4(d), respectively.

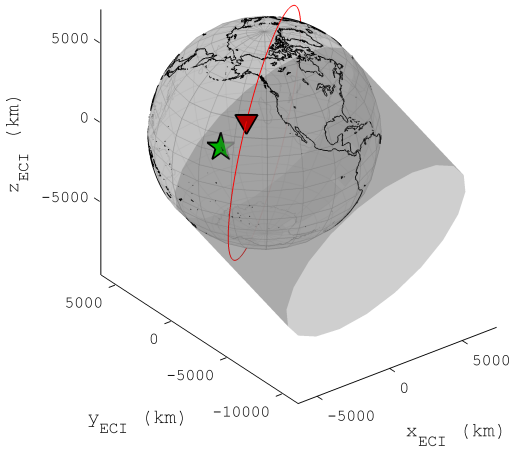

Figure 3: UCT 1 GeometryVisualization

Statistics on UCT 1 classification and prioritization parameters are compiled and presented in Tables 4 and 5. As can be seen, without assuming the SO is a member of the SOC, there is a 4.9% probability that the UCT 1 corresponds to a LEO:polar object. However, because the majority of SOC entries correspond to LEO:polar objects, under the assumption that the SO is a member of the SOC there is a 82.6% probability that UCT 1 possesses a LEO:polar orbit. As depicted in Figure 4(a), the majority of the admissible region volume corresponds to NOTA, HEO:NOTA, and MEO:low orbit classifications. Conversely, if SOC membership is assumed, then these volumes are substantially attenuated because of low SOC population densities in those regions.

Table 4: UCT 1: LEO:Polar UCT Classification Probabilities

Classification ($\mathcal{A}_i$)	Frequency	H_i $\mathbb{P}[\mathbf{X}_u \in \mathcal{A}_i \vert \mathcal{A}]$	$H_{i,ap}$ $\mathbb{P}[\mathbf{X}_u \in \mathcal{A}_i \vert \mathcal{A}, \text{SOC}]$
LEO:polar	**1403**	**0.0490**	**0.8264**
NOTA	15803	0.5524	0.1011
HEO:NOTA	9617	0.3362	0.0556
MEO:low	1785	0.0624	0.0169
Totals	28608	1.0000	1.0000

The prioritization parameter statistics shown in Table 5 give substantial information for potential multi-object prioritization schemes to ingest. Examining the 'Time Left to Detect' statistics, there is only a 91.5% probability that the object will still be detectable in 10 seconds. Altnernately, there is a 95% probability that the SO will remain detectable for 2.99 seconds. There is a very high probability (nearly 100%) that the UCT will not approach within 50km of the ISS. In fact, 95% of all trajectories in the admissible region have

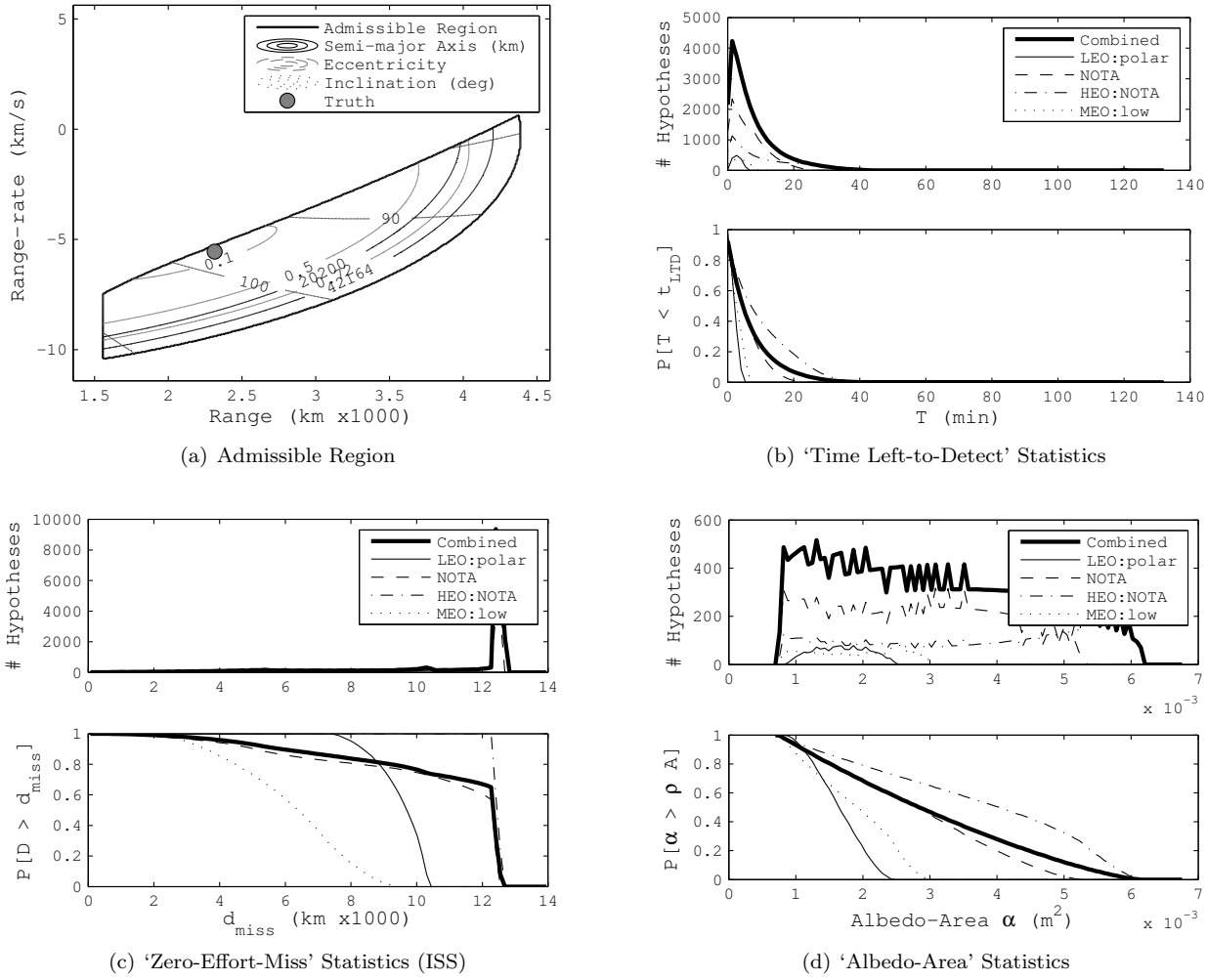

(a) Admissible Region

(b) 'Time Left-to-Detect' Statistics

(c) 'Zero-Effort-Miss' Statistics (ISS)

(d) 'Albedo-Area' Statistics

Figure 4: UCT 1: Polar Orbiting LEO Admissible Region and Prioritization Parameter Satistics

a closest approach in excess of 4,346km. The albedo-area results in Table 5 suggest that, with an apparent magnitude of 13, for all orbit classifications the object has either a low albedo, a small area, or both.

Table 5: UCT 1: LEO:Polar UCT Prioritization Parameter Statistics

Class. ($\mathcal{A}_i$)	$\mathbb{P}[t_{\text{LTD}} \geq 10s]$	t_{LTD} @ 95% Conf. (s)	$\mathbb{P}[d_{\text{ZEM}} > 50km]$	d_{ZEM} @ 95% Conf. (km)	$\mathbb{P}[\rho A > 0.2m^2]$	ρA @ 95% Conf. (m^2)
Combined	0.915	2.99	1.000	4346	0.000	0.000931
LEO:polar	**0.955**	**11.30**	**1.000**	**8012**	**0.000**	**0.001018**
NOTA	0.908	2.76	0.999	3682	0.000	0.000909
HEO:NOTA	0.927	3.47	1.000	12290	0.000	0.001000
MEO:low	0.873	1.99	1.000	2987	0.000	0.000847

5.4 UCT 2: Low Inclination Low-Earth Orbit (LILO) Object

Just as LEO:polar orbits are very common in the SOC, a particular orbit classification 'Low-Inlclination Low Earth Orbits' (LEO:LILOs) are known to be under-represented due to a lack of equatorial SSN assets.

This under-representation makes investigating the proposed classification, characterization, and prioritization methods on a LEO:LILO UCT worthwhile. UCT 2 is in fact generated by a LEO:LILO space object. The geometry of the true orbit is shown in Figure 5.

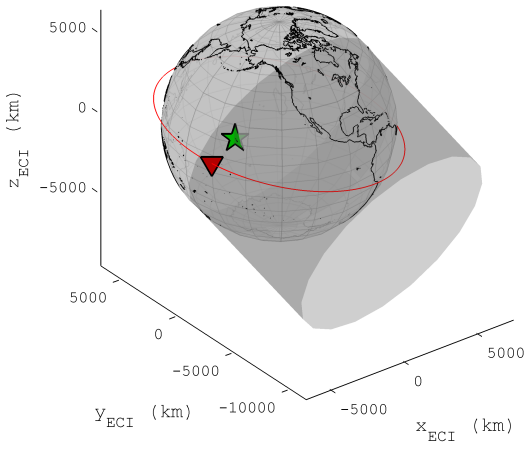

Figure 5: UCT 2 Geometry Visualization

The admissible region for UCT 2 is plotted in Figure 6(a), while the 'Time Left-to-Detect,' 'Zero-Effort Miss,' and 'Albedo-Area' statistics are depicted in Figures 6(b), 6(c), and 6(d), respectively.

An application of the classification methodology generates Table 6. Without assuming that UCT 2 is generated by an object belonging to the SOC, using only a single underdetermined detection there is a 4.2% probability that UCT 2 is generated by a LEO:LILO object. However, if it is assumed that UCT 2 is generated by a SOC member, then because there are so few LEO:LILO objects in the SOC, this probability is substantially attenuated (0.07%). This emphasizes a significant potential pitfall of assuming that a SO generating a UCT is a member of the SOC - the conclusion can only be as good as the *a-priori* assumptions, and in this case the SOC LEO:LILO population is very small (only 17 LEO:LILO SOs, as shown in Table 2).

Table 6: UCT 2: LEO:LILO UCT Classification Probabilities

Classification ($\mathcal{A}_i$)	Frequency	H_i $\mathbb{P}[\mathbf{X}_u \in \mathcal{A}_i \vert \mathcal{A}]$	$H_{i,ap}$ $\mathbb{P}[\mathbf{X}_u \in \mathcal{A}_i \vert \mathcal{A}, \text{SOC}]$
GTO:NOTA	20243	0.6454	0.9574
HEO:NOTA	9634	0.3072	0.0223
LEO:NOTA	171	0.0055	0.0196
LEO:LILO	**1315**	**0.0419**	**0.0007**
Totals	31363	1.0000	1.0000

The UCT 2 prioritization parameter statistics shown in Table 7 are informative, however. Examining the 'Time Left to Detect' statistics, there is a 96% probability that UCT 2 will continue to be detectable for an additional 10 seconds. One classification in particular, LEO:NOTA, is observable for an additional 66 seconds with a 95% confidence. As with UCT 1, is is highly unlikely that UCT 2 will approach within 50km of the ISS over the time interval examined. Also, with an apparent magnitude of 13, the combined Albedo-Area is rather small with 95% confidence.

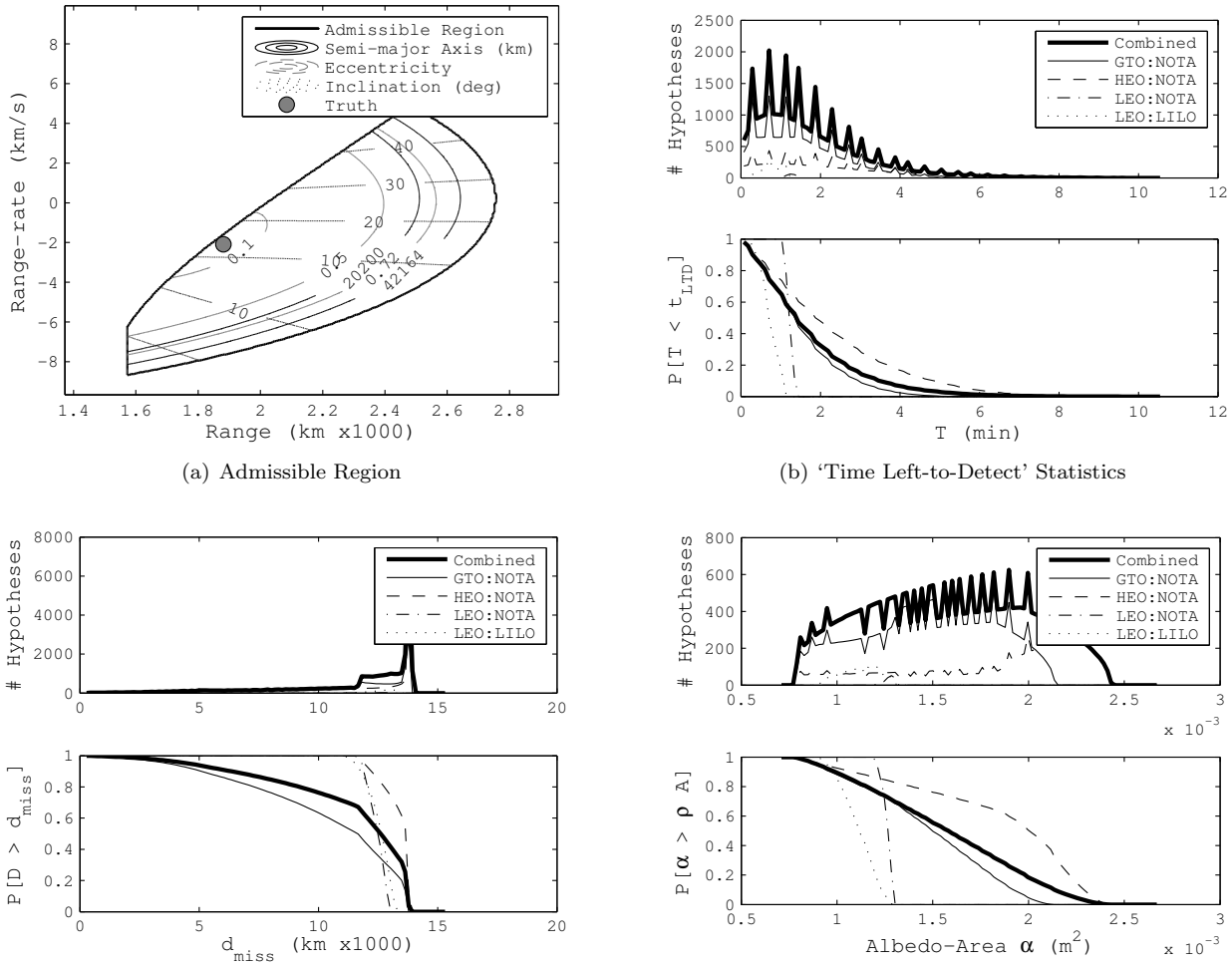

(a) Admissible Region

(b) 'Time Left-to-Detect' Statistics

(c) 'Zero-Effort-Miss' Statistics (ISS)

(d) 'Albedo-Area' Statistics

Figure 6: UCT 2: LEO LILO Admissible Region and Prioritization Parameter Satistics

Table 7: UCT 2: LEO:LILO UCT Prioritization Parameter Statistics

Class. ($\mathcal{A}_i$)	$\mathbb{P}[t_{\text{LTD}} \geq 10s]$	t_{LTD} @ 95% Conf. (s)	$\mathbb{P}[d_{\text{ZEM}} > 50km]$	d_{ZEM} @ 95% Conf. (km)	$\mathbb{P}[\rho A > 0.2m^2]$	ρA @ 95% Conf. (m^2)
Combined	0.960	11.65	1.000	4555	0.000	0.000898
GTO:NOTA	0.956	11.13	0.991	3684	0.000	0.000883
HEO:NOTA	0.962	12.18	1.000	11920	0.000	0.000929
LEO:NOTA	1.000	63.06	1.000	11820	0.000	0.001209
LEO:LILO	**1.000**	**18.13**	**1.000**	**11540**	**0.000**	**0.000948**

5.5 UCT 3: MEO Subsynchronous Object

Medium Earth Orbits (MEOs) contain 2:1 synchronous orbits, including the Global Positioning System (GPS) satellites. UCT 3 is generated by a SO in MEO:synchronous, as depicted in Figure 7. The admissible region generated by UCT 3 is shown in Figure 8(a). The prioritization parameter statistics plots for 'Time Left to Detect,' 'Zero-Effort Miss,' and 'Albedo-Area' are given in Figures 8(b), 8(c), and 8(d).

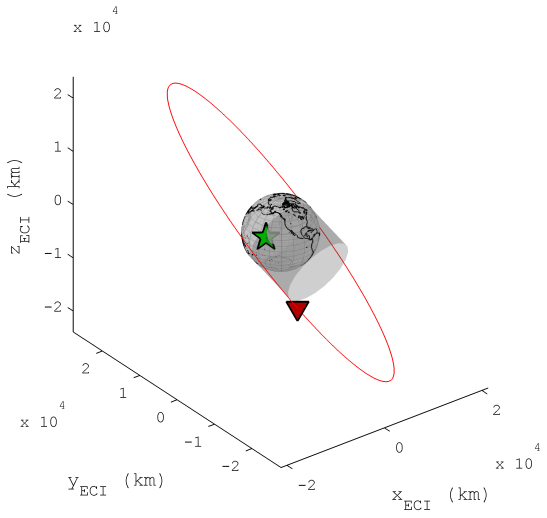

Figure 7: UCT 3 Geometry Visualization

Orbit classification results for UCT 3 with and without assuming SOC membership are summarized in Table 8. Here, it can be seen that the admissible region associated with MEO:subsynch orbits is rather small, generating a MEO:subsynch classification probability of only 1%. Interestingly, because there are not a large number of objects in MEO:subsynch orbits, assuming membership in the SOC reduces the probability of MEO:subsynch classification to 0.6%.

Table 8: UCT 3: MEO:subsynch UCT Classification Probabilities

		H_i	$H_{i,ap}$
Classification ($\mathcal{A}_i$)	Count	$\mathbb{P}\left[\mathbf{X}_u \in \mathcal{A}_i \vert \mathcal{A}\right]$	$\mathbb{P}\left[\mathbf{X}_u \in \mathcal{A}_i \vert \mathcal{A}, \text{SOC}\right]$
GTO:NOTA	7262	0.2364	0.8578
HEO:NOTA	19116	0.6224	0.1106
NOTA	3925	0.1278	0.0251
MEO:subsynch	**307**	**0.0100**	**0.0062**
MEO:NOTA	105	0.0034	0.0003
Totals	30715	1.0000	1.0000

The prioritization parameter statistics for UCT 3 are contained in Table 9. Here, it can be seen that substantial time remains to collect followup observations of UCT 3; it will be visible for 2,237 seconds (about 37 minutes) with 95% confidence. Similar to the other UCTs, UCT 3 is highly unlikely to pass within 50km of the ISS. Interestingly, the statistical data suggest that with an apparent magnitude of 13, UCT 3 has a moderately large Albedo-Area. Overall, there is a 36.5% probability that the albedo-area exceeds 0.2, which is a proxy threshold for identifying 'large' or 'bright' space objects.

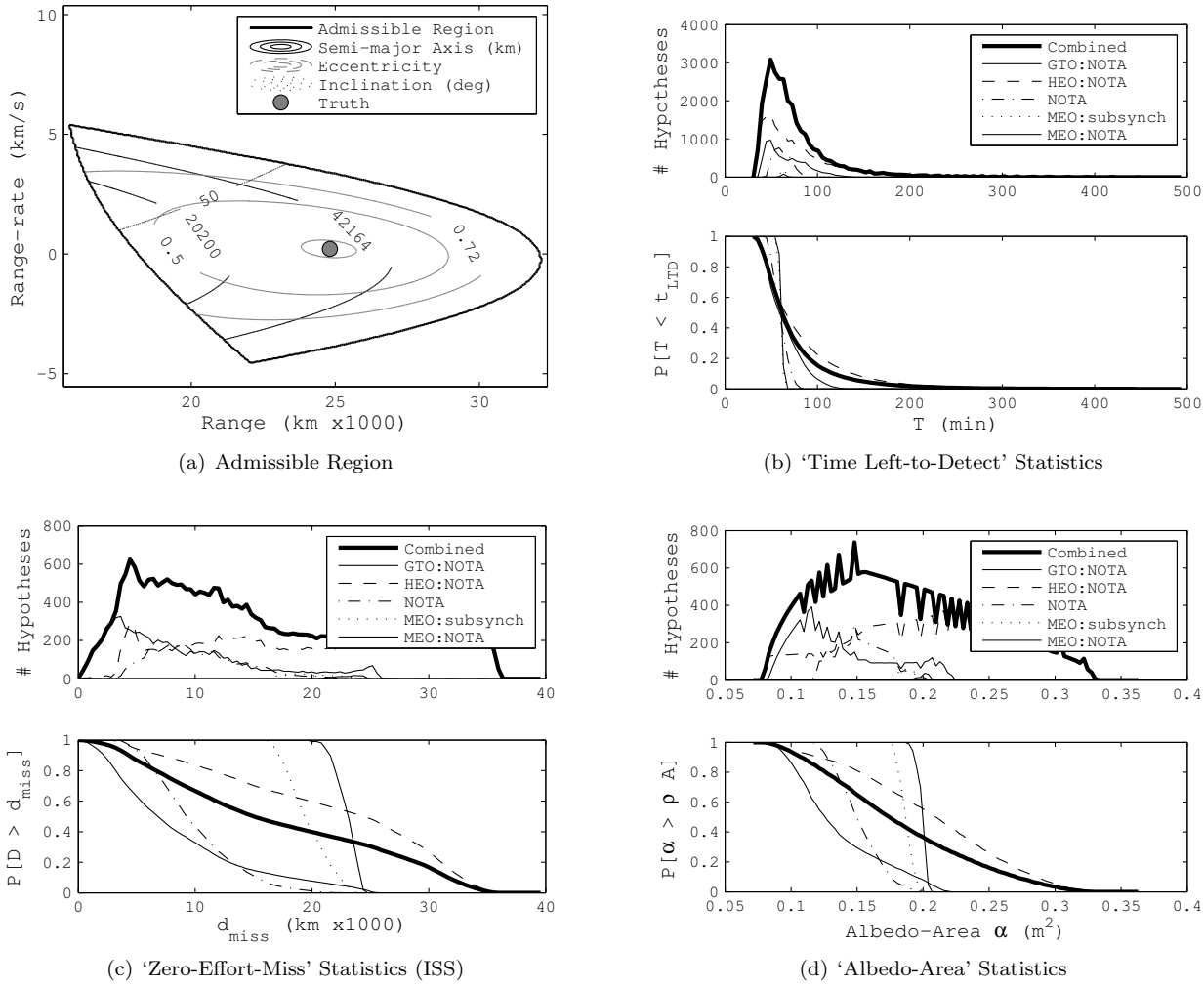

(a) Admissible Region

(b) 'Time Left-to-Detect' Statistics

(c) 'Zero-Effort-Miss' Statistics (ISS)

(d) 'Albedo-Area' Statistics

Figure 8: UCT 3: MEO Subsynchronous Admissible Region and Prioritization Parameter Satistics

Table 9: UCT 3: MEO:subsynch UCT Prioritization Parameter Statistics

Class. ($\mathcal{A}_i$)	$\mathbb{P}[t_{\text{LTD}} \geq 10s]$	t_{LTD} @ 95% Conf. (s)	$\mathbb{P}[d_{\text{ZEM}} > 50km]$	d_{ZEM} @ 95% Conf. (km)	$\mathbb{P}[\rho A > 0.2m^2]$	ρA @ 95% Conf. (m^2)
Combined	1.000	2237	0.999	3178	0.365	0.0970
GTO:NOTA	1.000	2340	1.000	1447	0.080	0.0919
HEO:NOTA	1.000	2165	1.000	4702	0.553	0.1002
NOTA	1.000	2784	1.000	4684	0.002	0.1234
MEO:subsynch	**1.000**	**3303**	**1.000**	**16780**	**0.007**	**0.1780**
MEO:NOTA	1.000	3361	1.000	21120	0.469	0.1917

5.6 UCT 4: GTO Object

The utility of geosynchronous orbits has resulted in a substantial population of SOs in Geosynchronous Transfer Orbits (GTOs). As seen in Table 2, fully 10% of all SOC objects are classified as possessing GTO orbits. The UCT 4 observation geometry is shown in Figure 9. Additionally, the Admissible Region is shown in Figure 10(a), while the prioritization parameter statistics for 'Time Left to Detect,' 'Zero-Effort Miss,' and 'Albedo-Area' are shown in Figures 10(b), 10(c), and 10(d).

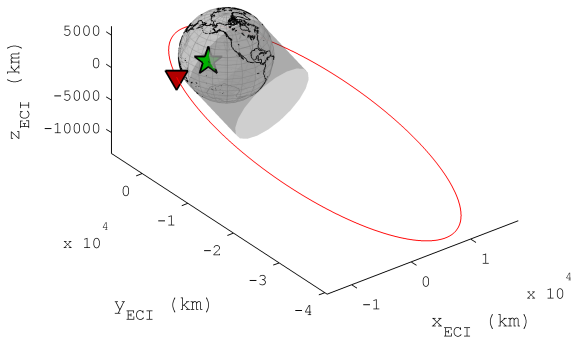

Figure 9: UCT 4 Geometry Visualization

Classification results using UCT 4 observations are tabulated in Table 10. Without *a-priori* information, the probability that UCT 4 is a GTO:NOTA object is 34.8%. When SOC membership is presumed, the probability of a GTO:NOTA classification jumps to 91.5%. Emphatically, this is due to the strong representation of GTO:NOTA objects in the SOC.

Table 10: UCT 4: GTO UCT Classification Probabilities

Classification ($\mathcal{A}_i$)	Count	H_i $\mathbb{P}[\mathbf{X}_u \in \mathcal{A}_i \vert \mathcal{A}]$	$H_{i,ap}$ $\mathbb{P}[\mathbf{X}_u \in \mathcal{A}_i \vert \mathcal{A}, \text{SOC}]$
GTO:NOTA	**9400**	**0.3477**	**0.9147**
HEO:NOTA	11897	0.4400	0.0567
NOTA	5200	0.1923	0.0274
MEO:NOTA	541	0.0200	0.0011
Totals	27038	1.0000	1.0000

Prioritization parameter statistics for UCT 4 are shown in Table 11. Here, UCT 4 should continue to be detectable for an additional 812 seconds (13.5 minutes) with 95% confidence. As with other UCTs, there is virtually no risk that UCT 4 will approach within 50km of the ISS. Also, with an apparent magnitude of 13, the albedo-area statistics suggest that this parameter is relatively small.

Table 11: UCT 4: GTO UCT Prioritization Parameter Statistics

Class. ($\mathcal{A}_i$)	$\mathbb{P}[t_{\text{LTD}} \geq 10s]$	t_{LTD} @ 95% Conf. (s)	$\mathbb{P}[d_{\text{ZEM}} > 50km]$	d_{ZEM} @ 95% Conf. (km)	$\mathbb{P}[\rho A > 0.2m^2]$	ρA @ 95% Conf. (m^2)
Combined	1.000	811.5	0.999	1728	0.000	0.0138
GTO:NOTA	**1.000**	**804.1**	**1.000**	**1019**	**0.000**	**0.0132**
HEO:NOTA	1.000	757.1	1.000	6718	0.000	0.0166
NOTA	1.000	1194.7	1.000	4006	0.000	0.0164
MEO:NOTA	1.000	1515.9	1.000	4842	0.000	0.0166

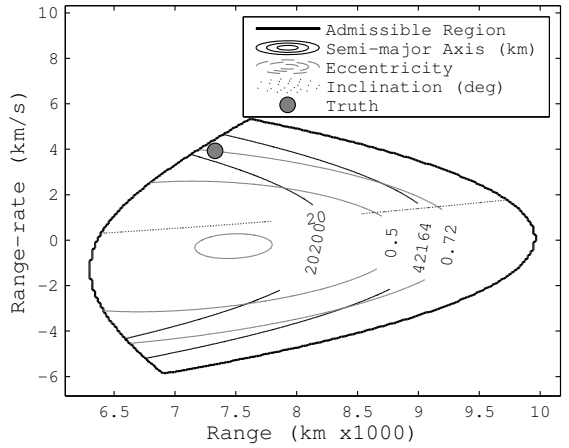

(a) Admissible Region

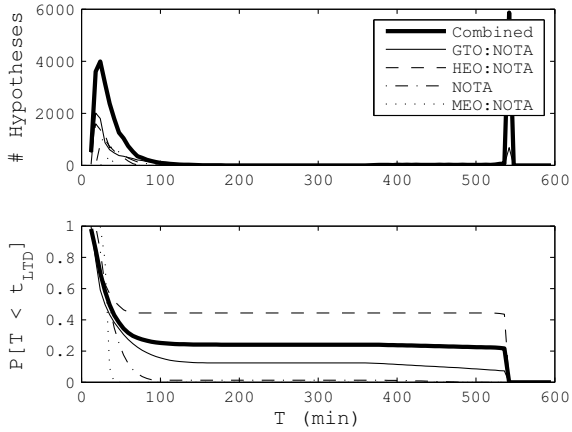

(b) 'Time Left-to-Detect' Statistics

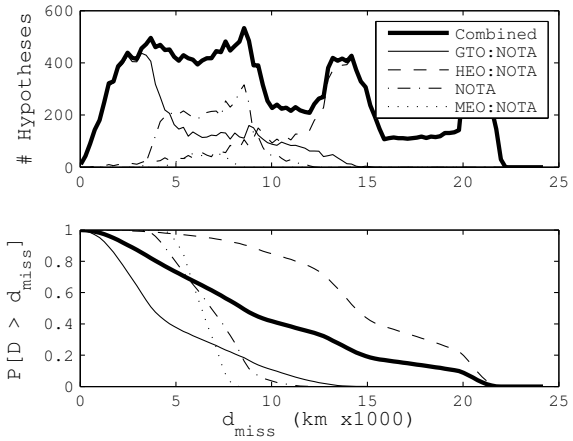

(c) 'Zero-Effort-Miss' Statistics (ISS)

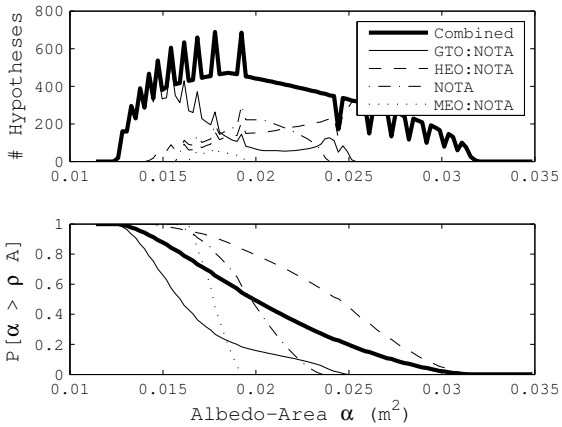

(d) 'Albedo-Area' Statistics

Figure 10: UCT 4: GTO Admissible Region and Prioritization Parameter Satistics

5.7 UCT 5: GEO Object

Space objects in geosynchronous orbit generate substantial economic value (e.g., communications satellites) and also represent a sizable population of large objects in the SOC (see Table 2). UCT 5 is generated by just such an object, and is visualized in Figure 11. The admissible region is given in Figure 12(a) and prioritization parameter statistics for 'Time Left to Detect,' 'Zero-Effort Miss Distance,' and 'Albedo-Area are shown in Figures 12(b), 12(c), and 12(d).

Table 12 presents the classification probabilities with and without assuming the SO is well represented by the SOC state distribution. Here, the principal shortcoming of the proposed approach (discussed in §2.2.5) is emphasized. As shown in Table 12, while the true SO orbit classification is GEO:slot, the classification approach does not identify a non-zero probability for this classification. The region of space in the admissible region (Figure 12(a)) that corresponds to orbits consistent with GEO:slot classifications is quite small, and is not effectively sampled with the discretization used in this example. However, as discussed in §2.2.5, there is a small region of orbits within the GEO:slot orbit classification that generate non-empty regions in the admissible region $\mathcal{A}$. Said differently, UCT 5 is consistent with the GEO:slot classification, however the probability cannot be calculated due to sampling fidelity.

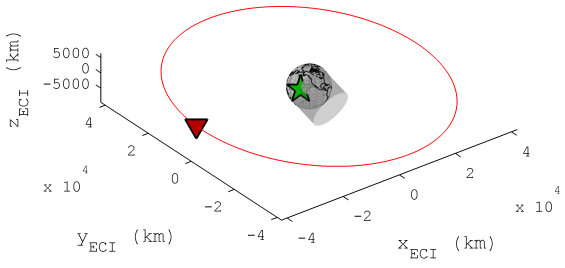

Figure 11: UCT 5 Geometry Visualization

Table 12: UCT 5: GEO UCT Classification Probabilities

		H_i	$H_{i,ap}$
Classification ($\mathcal{A}_i$)	Count	$\mathbb{P}[\mathbf{X}_u \in \mathcal{A}_i \vert \mathcal{A}]$	$\mathbb{P}[\mathbf{X}_u \in \mathcal{A}_i \vert \mathcal{A}, \text{SOC}]$
GTO:NOTA	7502	0.2409	0.8651
HEO:NOTA	23021	0.7391	0.1301
NOTA	587	0.0188	0.0037
GEO:NOTA	36	0.0012	0.0011
GEO:graveyard	2	0.0001	0.0000
GEO:slot	**0**	*	*
Totals	31148	1.0000	1.0000

The prioritization parameter statistics for UCT 5 are given in Table 13. Here, it is highly probable that UCT 5 will continue to permit detection for 5,064 seconds (84 minutes) with 95% confidence. As with other UCTs, it is highly probable that UCT 5 will not approach within 50km of the ISS. Interestingly, it is highly probable (93.4%) that UCT 5 is generated by a SO with an Albedo-Area in excess of 0.2, possibly indicating it is a large or very bright object.

Table 13: UCT 5: GEO UCT Prioritization Parameter Statistics

		t_{LTD} @ 95%		d_{ZEM} @ 95%		ρA @ 95%
Class. ($\mathcal{A}_i$)	$\mathbb{P}[t_{\text{LTD}} \geq 10s]$	Conf. (s)	$\mathbb{P}[d_{\text{ZEM}} > 50km]$	Conf. (km)	$\mathbb{P}[\rho A > 0.2m^2]$	Conf. (m^2)
Combined	1.000	5064	1.000	3355	0.934	0.193
GTO:NOTA	1.000	5846	1.000	1590	0.858	0.183
HEO:NOTA	1.000	4774	1.000	6503	0.957	0.205
NOTA	1.000	9306	1.000	3986	1.000	0.233
GEO:NOTA	1.000	32110	1.000	33280	1.000	0.419
GEO:graveyard	1.000	32110	1.000	35020	1.000	0.431
GEO:slot	*	*	*	*	*	*

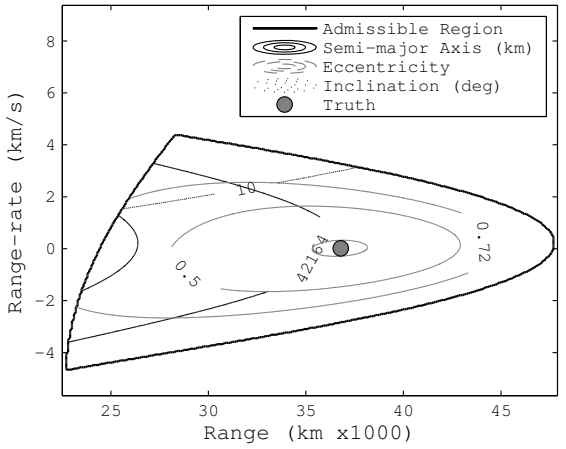

(a) Admissible Region

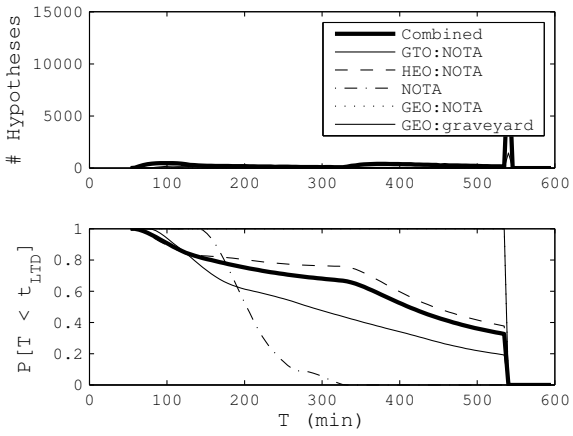

(b) 'Time Left-to-Detect' Statistics

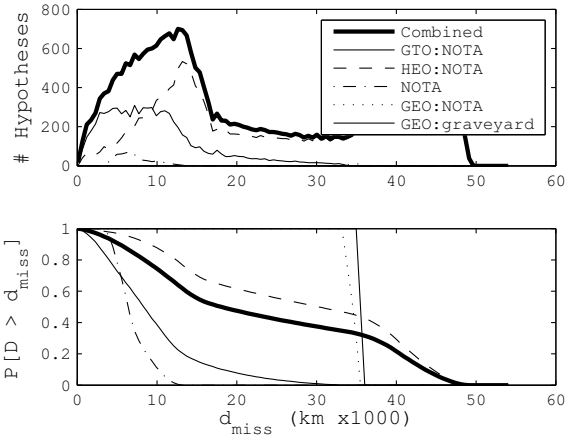

(c) 'Zero-Effort-Miss' Statistics (ISS)

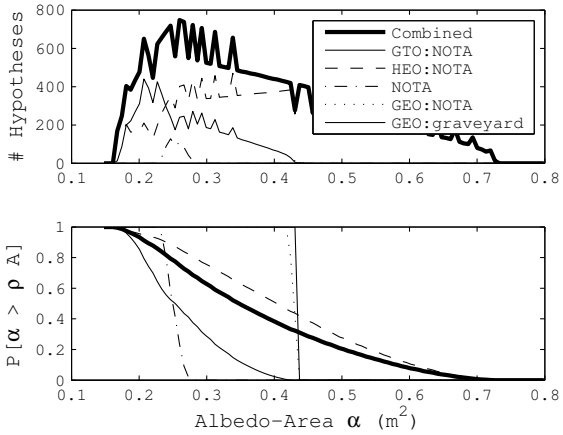

(d) 'Albedo-Area' Statistics

Figure 12: UCT 5: GEO Admissible Region and Prioritization Parameter Satistics

5.8 UCT 6: Molniya Object

As shown in Figure 13 the final track, UCT 6, is generated by a SO in Molniya orbit. The admissible region generated by UCT 6 is shown in Figure 14(a), while the 'Time Left to Detect,' 'Zero-Effort Miss,' and 'Albedo-Area prioritization parameter histograms and CDFs are given in Figures 14(b), 14(c), and 14(d), respectively.

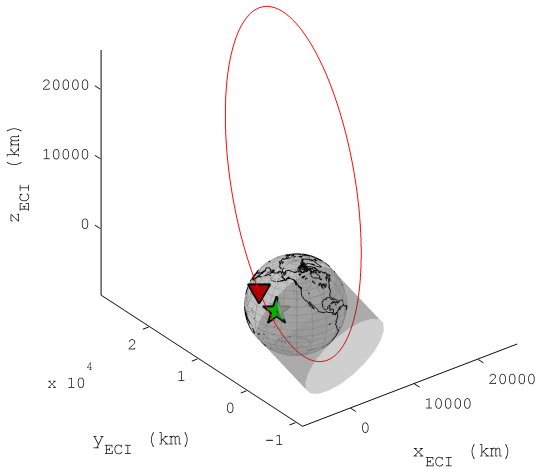

Figure 13: UCT 6 Geometry Visualization

The classification statistics for UCT 6 are summarized in Table 14. Without presuming that UCT 6 is generated by an object well represented by the SOC, the classification probability for Molniya:NOTA is 8.4%. However, because there is a dearth of objects with Molinya orbits in the SOC, the probability drops to 3.6% if the SOC is used as an *a-priori* distribution.

Table 14: UCT 6: Molniya UCT Classification Probabilities

		H_i	$H_{i,ap}$
Classification ($\mathcal{A}_i$)	Count	$\mathbb{P}[\mathbf{X}_u \in \mathcal{A}_i \vert \mathcal{A}]$	$\mathbb{P}[\mathbf{X}_u \in \mathcal{A}_i \vert \mathcal{A}, \text{SOC}]$
GTO:NOTA	9901	0.3737	0.8990
HEO:NOTA	10088	0.3807	0.0449
Molniya:NOTA	**2226**	**0.0840**	**0.0362**
NOTA	3888	0.1467	0.0191
MEO:NOTA	393	0.0148	0.0008
Totals	26496.0000	1.0000	1.0000

A number of prioritization parameter statistics for UCT 6 are given in Table 15. Using these statistics, it can be seen that UCT 6 should continue to be visible for a further 575 seconds (9.6 minutes) with 95% confidence, and that there is a minimal probability that UCT 6 will approach within 50km of the ISS over the time interval examined (greater than 842km with 95% confidence). Similarly, the 'Albedo-Area' statistics suggest that the object is relatively small and / or dark.

With the geometries, classification probabilities, and prioritization statistics for each of the simultaneously detected UCTs given, a discussion is now given regarding how this actionable information can be used to rigorously support prioritization decisions for SSN sensor observations.

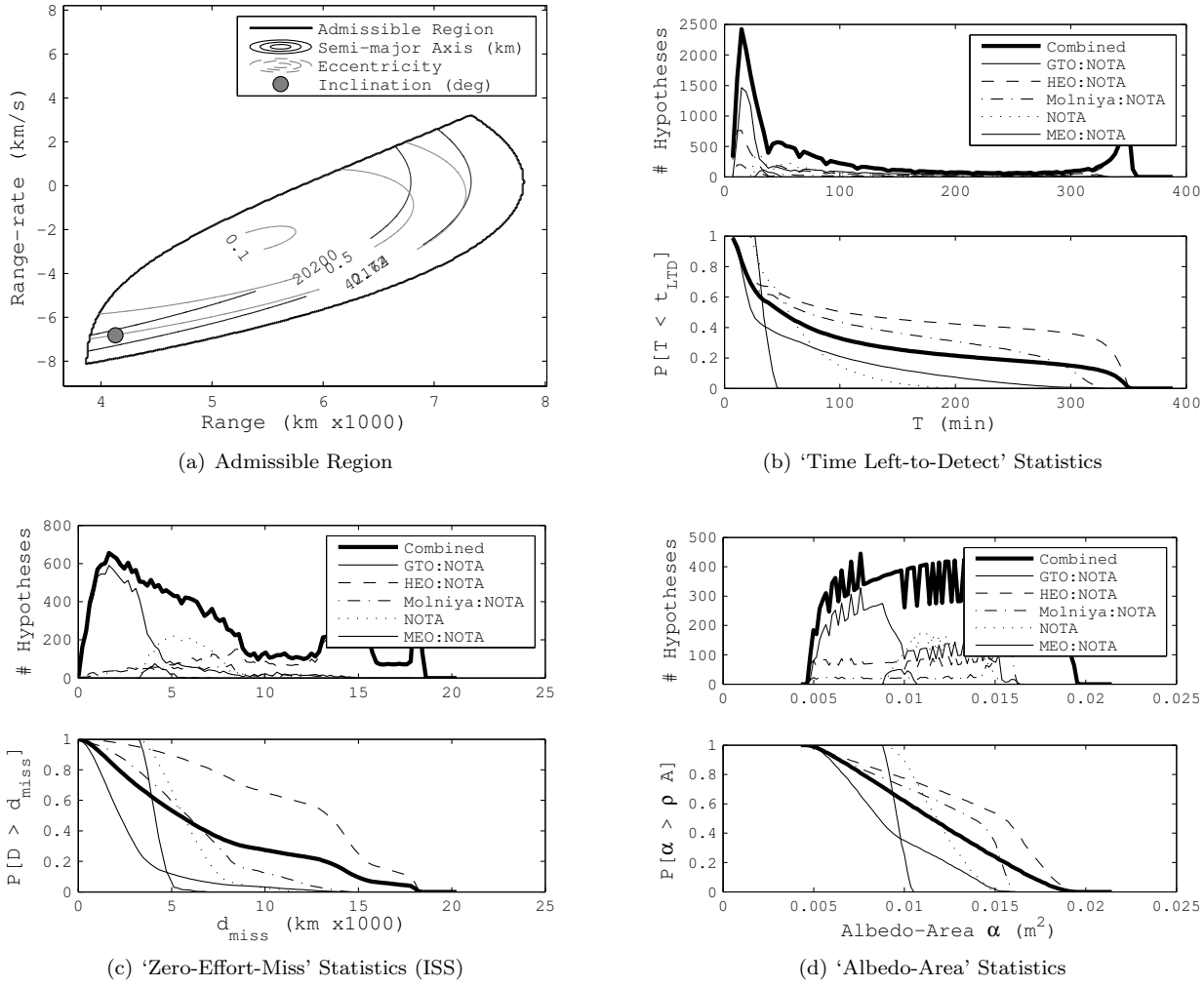

(a) Admissible Region

(b) 'Time Left-to-Detect' Statistics

(c) 'Zero-Effort-Miss' Statistics (ISS)

(d) 'Albedo-Area' Statistics

Figure 14: UCT 6: Molniya Admissible Region and Prioritization Parameter Satistics

Table 15: UCT 6: Molniya UCT Prioritization Parameter Statistics

Class. ($\mathcal{A}_i$)	$\mathbb{P}[t_{\text{LTD}} \geq 10s]$	t_{LTD} @ 95% Conf. (s)	$\mathbb{P}[d_{\text{ZEM}} > 50km]$	d_{ZEM} @ 95% Conf. (km)	$\mathbb{P}[\rho A > 0.2m^2]$	ρA @ 95% Conf. (m^2)
Combined	1.000	575.2	0.998	842	0.000	0.00569
GTO:NOTA	1.000	601.6	1.000	479	0.000	0.00548
HEO:NOTA	1.000	497.8	1.000	3227	0.000	0.00580
Molniya:NOTA	**1.000**	**534.0**	**1.000**	**1317**	**0.000**	**0.00558**
NOTA	1.000	1491.4	1.000	3744	0.000	0.00957
MEO:NOTA	1.000	1633.2	1.000	3396	0.000	0.00891

5.9 Discussion of Results

The classification results are first discussed, followed by the prioritization parameter statistical information. In each discussion several broad observations regarding SSN sensor prioritization are made. The classification probabilities for all UCTs without *a-priori* information are summarized in Table 16. Here, for each UCT, the orbit classification probability is explicitly stated. Importantly, it should be noted that the majority of classification probabilities are empty for each UCT, indicating that these classifications have been effectively

ruled out using the classification method. For those classifications with non-zero probability, the method is quite consistent in recovering orbit classifications reflecting the true SO orbit type (with the exception of the GEO:slot classification for UCT 5 as discussed in §5.5.7. As summarized in Table 17, when the classification is conditioned on SOC orbit densities, these probabilities are either magnified or attenuated depending on how well represented a given orbit type is in the SOC. For common orbit types, such as LEO:polar and GTO:NOTA orbits, this effect substantially increases the correct classification probability. However, for underrepresented orbit classifications (such as LEO:LILO, which is known to be under-sampled), conditioning the probabilities on the SOC distribution severely reduces correct classification probabilities.

If the objective of the SSN is to discover and track SOs from underrepresented orbit classifications, such as LEO:LILO, then the classification should not be conditioned on the existing SOC. Conversely, if the objective is to detect and track newly generated objects in a well represented classification (perhaps resulting from a LEO:polar object breakup), then conditioning the classification on the SOC may be a sensible approach. Additionally, whether the classification is conditioned or not, the relative classification probabilities in Tables 16 and 17 may still be useful when prioritization decisions must be made; perhaps the operator has no interest in HEO:NOTA objects, and wishes to focus SSN sensor assets on other categorizations.

Table 16: Classification Statistics Summary: No A-Priori Information

Classification ($\mathcal{C}_i$)	UCT 1: LEO:Polar	UCT 2: LEO:LILO	UCT 3: MEO:subsynch	UCT 4: GTO:NOTA	UCT 5: GEO:slot	UCT 6: Molniya
LEO:polar	**0.0490**	-	-	-	-	-
LEO:LILO	-	**0.0419**	-	-	-	-
LEO:NOTA	-	0.0055	-	-	-	-
Molniya:NOTA	-	-	-	-	-	**0.0840**
GTO:NOTA	-	0.6454	0.2364	**0.3477**	0.2409	0.3737
MEO:low	0.0624	-	-	-	-	-
MEO:subsynch	-	-	**0.0100**	-	-	-
MEO:NOTA	-	-	0.0034	0.0200	-	0.0148
GEO:slot	-	-	-	-	*	-
GEO:graveyard	-	-	-	-	0.0001	-
GEO:NOTA	-	-	-	-	0.0012	-
HEO:NOTA	0.3362	0.3072	0.6224	0.4400	0.7391	0.3807
NOTA	0.5524	-	0.1278	0.1923	0.0188	0.1467

Finally, the prioritization parameter statistics for the combined distributions generated by all UCTs are given in Table 18. Using this actionable information an operator may make prioritization decisions for UCT sensor tasking. For example, if the operator is concerned with detecting and initiating tracks on as many SOs as possible, it may be best to task sensors to follow-up on UCT 1 and UCT 2 before they are no longer detectable (3.0 s and 11.7s with 95% confidence). None of the UCTs pose a credible collision risk with the ISS over the time horizons considered; even the UCT with the closest approaches will pass in excess of 842km away with 95% confidence. Lastly, if the operator is interested in only tracking potentially larger or brighter objects, then based on the rigorously derived statistical information in Table 18, additional SSN sensor tasking for UCT 5 and UCT 3 may provide best results. Conversely, if the operator wishes to track SOs that are smaller or darker, then perhaps UCT 1 and UCT 2 should be observed further.

Table 17: Classification Statistics Summary: With A-Priori Information

Classification ($\mathcal{C}_i$)	UCT 1: LEO:Polar	UCT 2: LEO:LILO	UCT 3: MEO:subsynch	UCT 4: GTO:NOTA	UCT 5: GEO:slot	UCT 6: Molniya
LEO:polar	**0.8264**	-	-	-	-	-
LEO:LILO	-	**0.0007**	-	-	-	-
LEO:NOTA	-	0.0223	-	-	-	-
Molniya:NOTA	-	-	-	-	-	**0.0362**
GTO:NOTA	-	0.9674	0.8578	**0.9147**	0.8651	0.8990
MEO:low	0.0169	-	-	-	-	-
MEO:subsynch	-	-	**0.0062**	-	-	-
MEO:NOTA	-	-	0.0003	0.0011	-	0.0008
GEO:slot	-	-	-	-	*	-
GEO:graveyard	-	-	-	-	0.0000	-
GEO:NOTA	-	-	-	-	0.0011	-
HEO:NOTA	0.0556	0.0223	0.1106	0.0567	0.1301	0.0449
NOTA	0.1011	-	0.0251	0.0274	0.0037	0.0191

Table 18: Prioritization Parameter Statistics: A Comparison

UCT #	True Class. ($\mathcal{C}_i$)	$\mathbb{P}[t_{\text{LTD}} \geq 10s]$	t_{LTD} @ 95% Conf. (s)	$\mathbb{P}[d_{\text{ZEM}} > 50km]$	d_{ZEM} @ 95% Conf. (km)	$\mathbb{P}[\rho A > 0.2m^2]$	ρA @ 95% Conf. (m^2)
1	LEO:polar	0.915	2.99	1.000	4346	0.000	0.000931
2	LEO:LILO	0.960	11.65	1.000	4555	0.000	0.000898
3	MEO:subsynch	1.000	2237	0.999	3178	0.365	0.0970
4	GTO:NOTA	1.000	811.5	0.999	1728	0.000	0.0138
5	GEO:slot	1.000	5064	1.000	3355	0.934	0.193
6	Molniya	1.000	575.2	0.998	842	0.000	0.00569

6 Conclusions

A Bayesian approach using admissible regions is proposed to classify space object orbits based only on incomplete state information derived directly from single sensor detections. The classification methodology is also extended to allow *a-priori* assumed classification distributions (e.g., from the Space Object Catalog) to be used in the classification activity. Further, a prioritization parameter approach wherein general functional mappings of sensor data and the hypothesized state can be used to infer parameters or properties of newly detected space objects is proposed. Hypotheses can be formed and rigorously tested using the resulting prioritization parameter distributions, enabling operators to define multiple decision criterion with which to prioritize future sensor tasking. Combined, classification and prioritization parameter statistics constitute actionable information that may be ingested by operators or autonomous algorithms to prioritize SSA resource allocation. Several example classifications and prioritization parameters are proposed and used in the simulated results section. A scenario involving six simultaneous UCT detections is used to motivate and discuss the algorithm performance and potential prioritization schemes.

Acknowledgements

This effort was partially funded by the American Society for Engineering Education (ASEE) Summer Faculty Fellowship Program (SFFP) and the Air Force Research Laboratory, Directed Energy Directorate, Kihei, HI.

References

[1] Rumsfeld, D. H., "Commission to Assess United States National Security Space Management and Organization," Tech. rep., Committee on Armed Services of the U.S. House of Representatives, January 2001.

[2] Joint Chiefs of Staff, "Space Operations," Joint Publication 3-14, May 2013.

[3] Wasson, M., "Space Situational Awareness in the Joint Space Operations Center," *Advanced Maui Optical and Space Surveillance Technologies Conference*, Wailea, HI, September 2011.

[4] Joint Functional Component Command for Space, "Space Track," `https://www.space-track.org`, June 2014.

[5] Committee for the Assessment of the US Air Forces Astrodynamic Standards and Aeronautics and Space Engineering Board and Division on Engineering and Physical Sciences and National Research Council (US), *Continuing Kepler's Quest: Assessing Air Force Space Command's Astrodynamics Standards*, National Academies Press, Washington, D.C., September 2012.

[6] Blackman, S., "Multiple hypothesis tracking for multiple target tracking," *Aerospace and Electronic Systems Magazine, IEEE*, Vol. 19, No. 1, Jan 2004, pp. 5–18.

[7] Mahler, R. P. S., *Statistical multisource-multitarget information fusion*, Vol. 685, Artech House, Norwood, MA, 2007.

[8] Wang, Y., Hussein, I., and Erwin, R. S., "Risk-Based Sensor Management for Integrated Detection and Estimation," *Journal of Guidance, Control, and Dynamics*, Vol. 34, No. 6, 2014/06/12 2011, pp. 1767–1778.

[9] Williams, P. S., Spencer, D. B., and Erwin, R. S., "Coupling of Estimation and Sensor Tasking Applied to Satellite Tracking," *Journal of Guidance, Control, and Dynamics*, Vol. 36, No. 4, 2014/06/12 2013, pp. 993–1007.

[10] Hussein, I., DeMars, K., Fruh, C., Erwin, R., and Jah, M., "An AEGIS-FISST integrated detection and tracking approach to Space Situational Awareness," *Information Fusion (FUSION), 2012 15th International Conference on*, IEEE, Singapore, July 2012, pp. 2065–2072.

[11] Sengupta, J. K., Tintner, G., and Morrison, B., "Stochastic Linear Programming with Applications to Economic Models," *Economica*, Vol. 30, No. 119, 1963, pp. 262–276.

[12] de Veciana, G. and Walrand, J., "Effective bandwidths: Call admission, traffic policing and filtering for ATM networks," *Queueing Systems*, Vol. 20, No. 1-2, 1995, pp. 37–59.

[13] Fukuda, T., Morimoto, Y., Morishita, S., and Tokuyama, T., "Data Mining Using Two-dimensional Optimized Association Rules: Scheme, Algorithms, and Visualization," *SIGMOD Rec.*, Vol. 25, No. 2, June 1996, pp. 13–23.

[14] Smith III, J. F., "Fuzzy logic resource manager: decision tree topology, combined admissible regions, and the self-morphing property," *Proc. SPIE 5096, Signal Processing, Sensor Fusion, and Target Recognition XII*, Vol. 5096, 2003, pp. 104–114.

[15] Milani, A., Gronchi, G. F., Vitturi, M. d., and Knezevic, Z., "Orbit determination with very short arcs. I admissible regions," *Celestial Mechanics and Dynamical Astronomy*, Vol. 90, No. 1-2, 2004, pp. 57–85.

[16] Tommei, G., Milani, A., and Rossi, A., "Orbit determination of space debris: admissible regions," *Celestial Mechanics and Dynamical Astronomy*, Vol. 97, No. 4, 2007, pp. 289–304.

[17] Holzinger, M. J., "Using Magnetometers for Space Object Characterization in Space Situational Awareness Applications," *Journal of Guidance, Control, and Dynamics*, (accepted) 2014.

[18] Maruskin, J. M., Scheeres, D. J., and Alfriend, K. T., "Correlation of Optical Observations of Objects in Earth Orbit," *Journal of Guidance, Control, and Dynamics*, Vol. 32, No. 1, January–February 2009, pp. 194–209.

[19] Fujimoto, K. and Scheeres, D. J., "Correlation of optical observations of earth-orbiting objects and initial orbit determination," *Journal of guidance, control, and dynamics*, Vol. 35, No. 1, January-February 2012, pp. 208–221.

[20] DeMars, K., Jah, M., and Schumacher, P., "Initial Orbit Determination using Short-Arc Angle and Angle Rate Data," *Aerospace and Electronic Systems, IEEE Transactions on*, Vol. 48, No. 3, July 2012, pp. 2628–2637.

[21] Fujimoto, K. and Scheeres, D. J., "Correlation of Multiple Singular Observations and Initial State Estimation by Means of Probability Distributions of High Codimension," *American Control Conference*, San Francisco, CA, July 2011, pp. 2387–2392.

[22] Mulrooney, M. K., Matney, M. J., Hejduk, M. D., and Barker, E. S., "An Investigation of Global Albedo Values," *Proceedings of the Advanced Maui Optical and Space Surveillance Technologies Conference*, 2008.

[23] Defense Advanced Research Projects Agency, "Uncued Detection of Low Inclined Low Earth Orbit Objects (LILO)," Special Notice DARPA-SN-14-09, 2014.